

WING STRUCTURAL CHARACTERISTICS OF A MEDIUM-RANGE
TRANSPORT AIRCRAFT

82758

A THESIS SUBMITTED TO
THE GRADUATE SCHOOL OF NATURAL AND APPLIED SCIENCES
OF
THE MIDDLE EAST TECHNICAL UNIVERSITY

BY

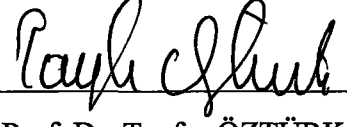
MELİN ŞAHİN

IN PARTIAL FULFILLMENT OF THE REQUIREMENTS FOR THE DEGREE
OF MASTER OF SCIENCE
IN
THE DEPARTMENT OF AERONAUTICAL ENGINEERING

TC. YÜKSEK ÖĞRETİM BAKANLIĞI
DOKÜMAN NO: ...

SEPTEMBER 1999

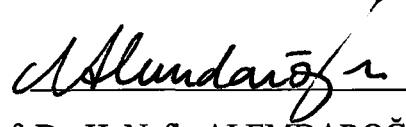
Approval of the Graduate School of Natural and Applied Sciences.



Prof. Dr. Tayfur ÖZTÜRK

Director

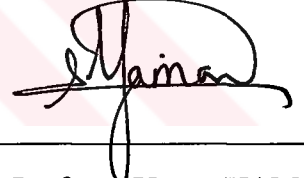
I certify that this thesis satisfies all the requirements as a thesis for the degree of Master of Science.



Prof. Dr. H. Nafiz ALEMDAROĞLU

Head of Department

This is to certify that I have read this thesis and that in my opinion it is fully adequate, in scope and quality, as a thesis for the degree of Master of Science.



Assoc. Prof. Dr. Yavuz YAMAN

Supervisor

Examining Committee Members

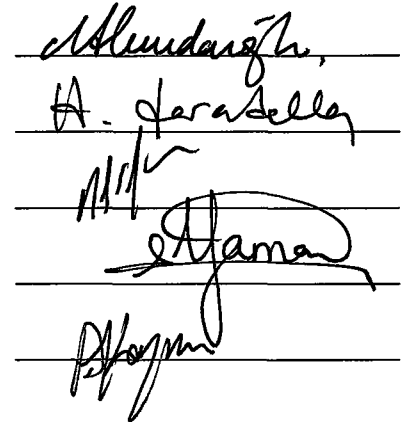
Prof. Dr. H. Nafiz ALEMDAROĞLU

Assoc. Prof. Dr. Haluk DARENDELİLER

Assoc. Prof. Dr. Mehmet Ş. KAVSAOĞLU

Assoc. Prof. Dr. Yavuz YAMAN

Dr. Altan KAYRAN



ABSTRACT

WING STRUCTURAL CHARACTERISTICS OF A MEDIUM-RANGE TRANSPORT AIRCRAFT

ŞAHİN, Melin

M. S., Department of Aeronautical Engineering

Supervisor: Assoc. Prof. Dr. Yavuz YAMAN

September 1999, 99 pages

In this thesis, wing structural characteristics of a medium-range transport aircraft are investigated by using a finite element package called I-DEAS. The three dimensional solid model of the wing is constructed and thereafter by using one and two dimensional finite elements, a mixed mesh is generated on the model. After the application of the boundary conditions, the dynamic and static analyses are performed and the solutions for the wing are obtained for with and without fuel cases. The results are presented in terms of the natural frequencies and mode shapes for the dynamic analysis and the displacements and stresses for the static analysis. These results are further analyzed in order to find the effect of the fuel and to investigate the behavior of the wing.

Keywords: Solid modeling, 3-D FEM, Dynamic analysis, Static analysis

ÖZ

ORTA MENZİLLİ BİR NAKLİYE UÇAĞININ KANAT YAPISAL ÖZELLİKLERİ

ŞAHİN, Melin

Yüksek Lisans, Havacılık Mühendisliği Bölümü

Tez Yöneticisi: Doç. Dr. Yavuz YAMAN

Eylül 1999, 99 sayfa

Bu tezde, I-DEAS adlı sonlu elemanlar paket programı kullanılarak orta menzilli bir nakliye uçağının kanat yapısal özellikleri incelenmiştir. Kanadın üç boyutlu katı modeli oluşturulmuş ve daha sonra bir ve iki boyutlu sonlu elemanlar kullanılarak model üzerinde karışık bir ağ yaratılmıştır. Sınır koşullarının uygulanmasından sonra statik ve dinamik analizler yapılmış ve kanadın yakıtlı ve yakıtsız durumları için çözümler elde edilmiştir. Sonuçlar dinamik analiz için doğal frekanslar ve titreşim biçim şekilleri, statik analiz için yerdeğiştirmeler ve gerilmeler şeklinde verilmiştir. Bu sonuçlar daha sonra yakıtın etkisini bulmak ve kanadın davranışını araştırmak için de kullanılmıştır.

Anahtar Kelimeler: Katı Modelleme, Üç Boyutlu Sonlu Elemanlar Yöntemi,
Dinamik Analiz, Statik Analiz



This work is dedicated to my mother, father and sweet sister.

Bu çalışma annem, babam ve tatlı kardeşime ithaf edilmiştir.

ACKNOWLEDGMENTS

I would like to express my gratitudes to Assoc. Prof. Dr. Yavuz YAMAN for his supervision, guidance, encouragement and patience during all the stages of this thesis.

I would also like to thank to Dr. Altan KAYRAN for his helpful comments and suggestions.

Finally, I would like to express all my love to my family for their support and patience.

TABLE OF CONTENTS

| | |
|--|-----|
| ABSTRACT..... | iii |
| ÖZ..... | iv |
| ACKNOWLEDGMENTS..... | vi |
| TABLE OF CONTENTS..... | vii |
| LIST OF TABLES..... | ix |
| LIST OF FIGURES..... | x |
| CHAPTER | |
| 1. INTRODUCTION..... | 1 |
| 1.1 Background to the Study | 1 |
| 1.2 Contents and Scope of this Study..... | 2 |
| 1.3 Limitations of the Study..... | 2 |
| 2. SOLID MODELING OF THE WING..... | 4 |
| 2.1 Introduction | 4 |
| 2.2 About I-DEAS | 4 |
| 2.3 Structural Elements Used in the Study | 5 |
| 2.3.1 Beam Elements..... | 6 |
| 2.3.2 Shell Elements | 7 |
| 2.3.3 Lumped Mass Element..... | 9 |
| 2.4 Solid Modeling of the Wing and Components..... | 10 |
| 2.4.1 Airfoil | 10 |
| 2.4.2 Skin..... | 11 |
| 2.4.3 Ribs | 13 |
| 2.4.4 Stiffeners | 16 |
| 2.4.5 Spars | 16 |

| | |
|---|----|
| 2.4.6 Leading and Trailing Edges..... | 17 |
| 2.4.7 Flap and Aileron..... | 20 |
| 3. MESHING OF THE WING MODEL..... | 25 |
| 3.1 Introduction | 25 |
| 3.2 Meshing with Different Elements..... | 26 |
| 3.2.1 Structural Parts Meshed by Beam Elements | 27 |
| 3.2.2 Structural Parts Meshed by Shell Elements | 33 |
| 4. DYNAMIC ANALYSIS OF THE WING..... | 46 |
| 4.1 About Dynamic Analysis Capabilities of I-DEAS..... | 46 |
| 4.2 Normal Mode Dynamic Analyses of the Wing..... | 47 |
| 4.2.1 Wing without Fuel | 47 |
| 4.2.2 Wing with Fuel | 55 |
| 5. STATIC ANALYSIS OF THE WING | 66 |
| 5.1 About Linear Static Analysis Capabilities of I-DEAS..... | 66 |
| 5.2 Application of g-Loading..... | 68 |
| 5.2.1 Analysis of the Wing Under Its Own Weight..... | 69 |
| 5.2.2 Analysis of the Wing Under Various g-Loading..... | 74 |
| 5.3 Determination of the Effective Transverse Stiffnesses of the Wing..... | 75 |
| 6. CONCLUSIONS..... | 89 |
| REFERENCES..... | 91 |
| APPENDICES | |
| Appendix A. Verification of dynamic analysis capabilities of I-DEAS..... | 92 |
| Appendix B. Presentation of hardware and modeling aspects | 97 |

LIST OF TABLES

TABLE

| | | |
|-----|---|----|
| 4.1 | Material properties of aluminum alloy used in the analysis..... | 48 |
| 4.2 | The natural frequencies for the wing without fuel..... | 48 |
| 4.3 | The natural frequencies for the wing with fuel | 58 |
| 4.4 | The percentage difference between the natural frequency of the wing with fuel and without fuel..... | 65 |
| 5.1 | The percentage difference between the maximum displacement and the maximum Von Mises stress for the wing with fuel and without fuel..... | 74 |
| 5.2 | Typical maximum g values for the aircraft..... | 74 |
| 5.3 | Effective stiffnesses of the wing..... | 82 |
| A.1 | Material properties of aluminium used in the analyses..... | 93 |
| A.2 | First ten theoretical natural frequencies of the beam..... | 93 |
| A.3 | First ten natural frequencies of the beam by using tetrahedron solid elements with element length of 2 (Number of nodes : 9058, Number of elements: 5309)..... | 94 |
| A.4 | First ten natural frequencies of the beam by using tetrahedron solid elements with element length of 3 (Number of nodes : 3045, Number of elements: 1600)..... | 94 |
| A.5 | First ten natural frequencies of the beam by using quadrilateral thin shell elements with element length of 1 (Number of nodes : 1111, Number of elements: 1000)..... | 95 |

| | | |
|-----|---|----|
| A.6 | First ten natural frequencies of the beam by using quadrilateral thin shell elements with element length of 3 (Number of nodes : 136, Number of elements: 99)..... | 95 |
| A.7 | First ten natural frequencies of the beam by using beam elements with element length of 1 (Number of nodes : 101, Number of elements: 100)..... | 96 |
| B.1 | Dynamic Analysis of the wing without fuel (First 20 modes)..... | 98 |
| B.2 | Dynamic Analysis of the wing with fuel (First 20 modes)..... | 98 |
| B.3 | Static Analysis of the wing under its own weight without fuel..... | 98 |
| B.4 | Static Analysis of the wing under its own weight with fuel..... | 99 |



LIST OF FIGURES

FIGURE

| | | |
|------|---|----|
| 2.1 | A linear beam element..... | 6 |
| 2.2 | A linear quadrilateral thin shell element..... | 8 |
| 2.3 | A linear triangle thin shell element..... | 9 |
| 2.4 | The symbol of lumped mass element..... | 10 |
| 2.5 | NACA 65 ₃ -218 airfoil used for the wing..... | 11 |
| 2.6 | Isometric view of the wing..... | 12 |
| 2.7 | Top view of the wing..... | 12 |
| 2.8 | Side view of the wing..... | 13 |
| 2.9 | Isometric view of the center wing ribs..... | 14 |
| 2.10 | View of a rib of the center wing..... | 14 |
| 2.11 | Isometric view of the outer wing ribs..... | 15 |
| 2.12 | View of a rib of the outer wing | 15 |
| 2.13 | Various stiffener profiles..... | 16 |
| 2.14 | Front and rear spar of the wing | 18 |
| 2.15 | Center wing leading edge (ribs and spar) | 19 |
| 2.16 | Center wing trailing edge..... | 20 |
| 2.17 | Outer wing leading edge (ribs and spar) | 21 |
| 2.18 | Outer wing trailing edge (ribs and spar) | 22 |
| 2.19 | Center wing flap (inboard flap) | 22 |
| 2.20 | Outer wing flap (outboard flap) | 23 |
| 2.21 | Aileron..... | 23 |
| 2.22 | Isometric view of the whole wing and structural components..... | 24 |
| 3.1 | The mesh and the calculated principal axes for a beam section.... | 28 |

| | | |
|------|--|----|
| 3.2 | Beam element used as a stiffener for the center wing and the solid view of the element..... | 29 |
| 3.3 | Beam elements used as stiffeners for the outer wing and the solid view of the elements | 30 |
| 3.4 | Locations of the center wing upper stiffeners..... | 31 |
| 3.5 | Locations of the outer wing upper stiffeners..... | 31 |
| 3.6 | Beam element used as a flange for the center and outer wing spar and solid view of the element..... | 32 |
| 3.7 | The orientation of the stiffeners under the skin of the center wing..... | 33 |
| 3.8 | Mesh of the leading edge rib and the anchor nodes..... | 35 |
| 3.9 | Mesh of the upper skin of the center wing..... | 36 |
| 3.10 | Mesh of the lower skin of the center wing..... | 36 |
| 3.11 | Mesh of the lower skin of the outer wing..... | 37 |
| 3.12 | Mesh of the upper skin of the outer wing | 38 |
| 3.13 | Isometric view of the center wing ribs with meshing..... | 39 |
| 3.14 | A view of a rib of the center wing with meshing | 40 |
| 3.15 | A view of a rib of the outer wing with meshing..... | 40 |
| 3.16 | Isometric view of the outer wing ribs with meshing..... | 41 |
| 3.17 | Mesh of the outer wing front and rear spars | 42 |
| 3.18 | Mesh of the leading edge skin..... | 43 |
| 3.19 | Mesh of the leading edge rib and part of the spar | 43 |
| 3.20 | Mesh of the inboard and outboard flaps and the aileron trailing edges..... | 44 |
| 3.21 | Solid view of the mesh of the center wing torque-box with stiffeners..... | 45 |
| 4.1 | Isometric view of the first bending about Y mode shape of the wing without fuel (Deformed and undeformed shapes) | 49 |
| 4.2 | Side view of the first bending about Y mode shape of the wing without fuel (Deformed and undeformed shapes) | 50 |
| 4.3 | Isometric view of the first bending about Z mode shape of the wing without fuel (Deformed and undeformed shapes) | 51 |

| | | |
|------|---|----|
| 4.4 | Top view of the first bending about Z mode shape of the wing without fuel (Deformed and undeformed shapes) | 52 |
| 4.5 | Isometric view of the second bending about Y mode shape of the wing without fuel (Deformed and undeformed shapes) | 53 |
| 4.6 | Side view of the second bending about Y mode shape of the wing without fuel (Deformed and undeformed shapes) | 54 |
| 4.7 | The location of the fuel and the station numbers of the ribs | 55 |
| 4.8 | The location of the lumped mass elements on a rib..... | 56 |
| 4.9 | The new mesh generated with lumped mass and shell elements (a rib with holes) | 57 |
| 4.10 | The new mesh generated with lumped mass and shell elements (a rib without any hole) | 57 |
| 4.11 | Isometric view of the first bending about Y mode shape of the wing with fuel (Deformed and undeformed shapes) | 59 |
| 4.12 | Side view of the first bending about Y mode shape of the wing with fuel (Deformed and undeformed shapes)..... | 60 |
| 4.13 | Isometric view of the first bending about Z mode shape of the wing with fuel (Deformed and undeformed shapes) | 61 |
| 4.14 | Top view of the first bending about Z mode shape of the wing with fuel (Deformed and undeformed shapes)..... | 62 |
| 4.15 | Isometric view of the second bending about Y mode shape of the wing with fuel (Deformed and undeformed shapes) | 63 |
| 4.16 | Side view of the second bending about Y mode shape of the wing with fuel (Deformed and undeformed shapes)..... | 64 |
| 5.1 | Isometric view of the total displacement pattern of the wing without fuel under its own weight..... | 70 |
| 5.2 | Isometric view of the Von Mises stress distribution of the wing without fuel under its own weight..... | 71 |
| 5.3 | Isometric view of the total displacement pattern of the wing with fuel under its own weight..... | 72 |
| 5.4 | Isometric view of the Von Mises stress distribution of the wing with fuel under its own weight | 73 |

| | | |
|------|---|----|
| 5.5 | G-loading vector components on isometric view of the wing..... | 74 |
| 5.6 | Isometric view of the total displacement pattern of the wing under various g-loading..... | 76 |
| 5.7 | Side view of the total displacement pattern of the wing under various g-loading..... | 77 |
| 5.8 | Top view of the total displacement pattern of the wing under various g loading..... | 78 |
| 5.9 | Isometric view of the Von Mises stress distribution of the wing under various g-loading..... | 79 |
| 5.10 | Isometric zoom view of the Von Mises stress distribution of the wing near root under various g-loading..... | 80 |
| 5.11 | Force versus displacement curve in Y direction..... | 81 |
| 5.12 | Force versus displacement curve in Z direction..... | 81 |
| 5.13 | Isometric view of the total displacement pattern of the wing under a force of $F_y = 10000$ N..... | 83 |
| 5.14 | Side view of the total displacement pattern of the wing under a force of $F_y = 10000$ N..... | 84 |
| 5.15 | Isometric view of the Von Mises stress distribution of the wing under a force of $F_y = 10000$ N..... | 85 |
| 5.16 | Isometric view of the total displacement pattern of the wing under a force of $F_z = 10000$ N..... | 86 |
| 5.17 | Top view of the total displacement pattern of the wing under a force of $F_z = 10000$ N..... | 87 |
| 5.18 | Isometric view of the Von Mises stress distribution of the wing under a force of $F_z = 10000$ N..... | 88 |
| A.1 | Beam used in the analyses and its dimensions..... | 92 |

CHAPTER 1

INTRODUCTION

1.1 Background to the Study

The analysis of aircraft structures is one of the most important and challenging issues that an aeronautical engineer faces. The methods of structural analysis are two types, namely analytical and numerical methods. Analytical methods provide closed-form solutions only at certain relatively simple cases and practically can not be used in the analysis of complex structures. The finite element method, which is a numerical procedure, is most widely used to solve various structural mechanics problems as a powerful and accurate analysis tool. The finite element method is capable of constructing three-dimensional models in order to simulate the characteristics of the real structure and using iterative methods for the solution.

In finite element applications, there is a solid model with arbitrary shape, under various loading with different boundary conditions. This model can be meshed by using different elements with different shapes and physical properties. The solution of the problem highly depends on the package program used during the analysis and the user who determines all the controlling parameters including the geometry, boundary conditions, element selection for meshing and solution method.

1.2 Contents and Scope of this Study

This thesis investigates the wing structural characteristics of a medium-range transport aircraft by using a finite element package called I-DEAS.

Chapter 2 gives a brief explanation about the package program capabilities for solid modeling and the elements used in the study. In that chapter, the methodology for constructing the three dimensional solid model of the wing is also explained.

Chapter 3 presents the generation of the mesh over the parts of the wing by using three different types of finite elements, namely the beam, shell and the lumped mass.

In the first part of Chapter 4, the dynamic analysis of the wing without any fuel is performed. In the second part of that chapter, the modeling of the effects of the fuel is explained and the dynamic characteristics of the wing having fuel are investigated. In the same chapter, in order to find the effect of the fuel on the response, the results of the two cases are also compared.

In Chapter 5, the static analyses are performed and the structural behavior of the wing is investigated.

Chapter 6 gives the general conclusions drawn from the analysis.

1.3 Limitations of the Study

This study aims to find the first three natural frequencies and the corresponding mode shapes for the dynamic analysis and also the displacements and stresses for the static analysis. The boundary condition is taken as cantilever in order not to complicate the model, since this is a comparative study for the analysis

of the wing with and without fuel cases. Although some of the skin of the aircraft wing control surfaces such as aileron or flaps are usually made of composite materials, the modeling of the composite layers with I-DEAS are beyond the scope and intention of this study. Therefore a typical aluminum alloy is used as a material for all the structural surfaces and components of the wing. During the analysis, the flap and the aileron configurations are chosen as being in undeflected position, hence the cruise condition is tried to be simulated.

As it is very well known one of the most important step of the analysis is the meshing of the wing. The finer the mesh the better the results approach usually increases the solution time and requires large memory. The solution for a model highly depends on the computer hardware performance and the capabilities. Therefore in order to get accurate results, the finite element package program and hardware capabilities must be well determined and the model must be solved by considering these limitations.

CHAPTER 2

SOLID MODELING OF THE WING

2.1 Introduction

This chapter explains the general procedure about the solid modeling of the wing. The tools used for the modeling of the structural parts of the wing are also described. Throughout this study, all analyses are performed by using a package program called I-DEAS [1].

2.2 About I-DEAS

I-DEAS which stands for Integrated Design Engineering and Analysis Software, is a general purpose program developed by Structural Dynamics Research Corporation (SDRC®). The program can solve a large variety of engineering problems. I-DEAS has different types of modules for specific applications such as design, simulation, drafting, test, manufacturing and management.

The program capabilities also include the finite element modeling and solution of linear and nonlinear static, normal and constraint mode dynamics, linear buckling, heat transfer, response dynamics and potential flow analyses. In

order to perform these analyses structural elements such as beam, shell or solid must be defined either on edges, surfaces or in volumes. Another step is the application of forces (in-plane, out-of plane, shear and distributed forces) and moments which are particularly necessary for linear and nonlinear static and buckling problems. These forces can be applied to selected edges, curves, sections, surfaces, nodes or to various locations on vertices, edges and surfaces during the analysis. A force on a node or geometric location is the combination of known forces and moments applied to the six nodal degrees of freedom (three displacements and three rotations) and the values for each force and moment refer to a selected coordinate system. Additionally, lumped mass, pressure in radial or normal directions can also be applied to the model. Various kinds of constraints can be applied to the model as boundary conditions. For example, displacement restraints are known as the displacements and rotations applied to selected edges, sections, surfaces, nodes, vertices or to locations on edges, curves, sections and surfaces. These restraints are valid for every analysis type. By changing the boundary conditions and using the elastic boundary conditions, the more realistic boundary conditions can also be simulated.

Detailed information about I-DEAS and the theoretical background of the finite element formulations used in various I-DEAS applications are given in [2].

2.3 Structural Elements Used in the Study

In this study three different structural elements namely beam, shell and a lumped mass which is a special element type are used with their appropriate options [3].

2.3.1 Beam Elements

In the analysis the linear beam element is used. This type of element is suitable for the structural analyses of linear static, nonlinear static, normal mode dynamics, constrained mode dynamics, linear buckling and heat transfer analysis.

When the topology of the beam is investigated, it can be seen that there are two nodes and one edge [4]. The element X axis is the beam centroidal axis and is directed from node 1 (the fore end) to node 2 (the aft end). The element Y and Z axes are the principal axes of the cross-section. Figure 2.1 illustrates typical beam element axes.

A beam element, unlike the other elements, is defined primarily by quantities derived from the shape of the beam rather than by the beam geometry itself. The linear beam element is straight and non-tapering. It is based on the Timoshenko beam theory, which includes transverse shear deformation. One can control the deformation due to transverse shear by shear area ratios. The shear deformation of a beam-like structure is relatively small for long and slender structural members but that increases as the structural member becomes shorter and stubbier. An Euler-Bernoulli beam representation can easily be obtained by entering shear area ratio of zero.

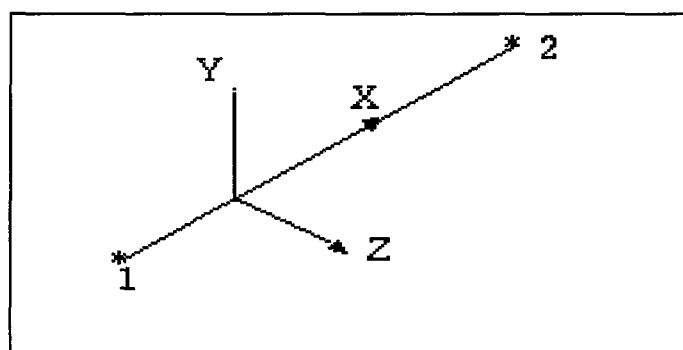


Figure 2.1 A linear beam element

The linear beam element has three translational DOF (Degree of Freedom) and three rotational DOF which are assigned to each node. The translations are in the direction of the nodal displacement coordinate system axes and have the dimension of length, on the other hand the rotations are about the nodal displacement coordinate system axes and are measured in radians.

The boundary conditions include loads, temperature restraints, and displacement restraints. The loads can be given at nodes as nodal forces and/or nodal moments or these forces and moments can be constantly or varyingly distributed along the beam element.

The beam cross-sectional properties, beam geometric data and the beam orientation will be discussed and explained in the meshing of the wing.

2.3.2 Shell Elements

The linear quadrilateral and triangle thin shell elements are selected for the analysis. These elements can be used for structural analyses of linear static, normal mode dynamics, constrained mode dynamics, linear buckling, nonlinear statics and heat transfer analysis and potential flow analysis.

The linear quadrilateral thin shell element has a topology of four nodes and four edges. The top surface of the element lies on the positive side denoted by n . The vector n is perpendicular to the shell mid-surface and is directed consistent with the right-hand rule system of nodal connectivity. Figure 2.2 shows a typical linear quadrilateral thin shell element.

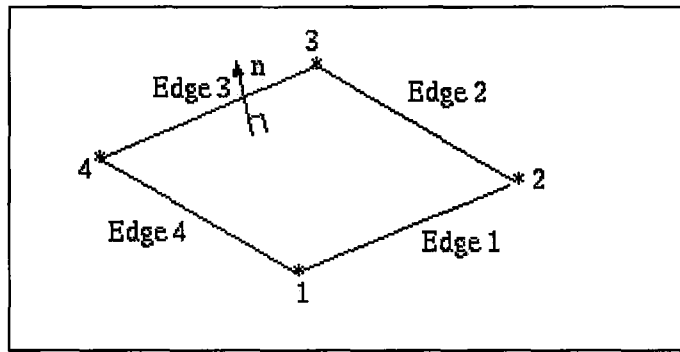


Figure 2.2 A linear quadrilateral thin shell element

Three translational and three rotational DOFs are assigned to each node of the linear quadrilateral thin shell element. The translations are in the direction of the nodal displacement coordinate system axes and have the dimension of length and the rotations are about the nodal displacement coordinate system axes and are measured in radians.

The boundary conditions for the element can be given as loads, temperature set, and displacement restraints. The loads may be applied in different forms. They can be nodal forces, nodal bending moments, face pressures, in-plane and/or out-of-plane loads, shear loads and edge bending moments. Nodal forces and nodal bending moments are directed in and about the nodal displacement coordinate system axes respectively.

The linear triangle thin shell element on the other hand has a topology of three nodes and three edges. The top surface of the element lies on the positive side denoted by n . The vector n is perpendicular to the shell mid-surface and is directed consistent with the right-hand rule system of nodal connectivity. Figure 2.3 represents a typical linear triangle thin shell element. Three translational and three rotational DOFs are assigned to each node of the linear triangle thin shell element. The other specifications related with the boundary conditions and mechanical loads which include nodal forces and bending moments are the same as the linear quadrilateral thin shell element. This element performs very well in bending. The

physical properties including the element thickness will be considered in the meshing of the wing.

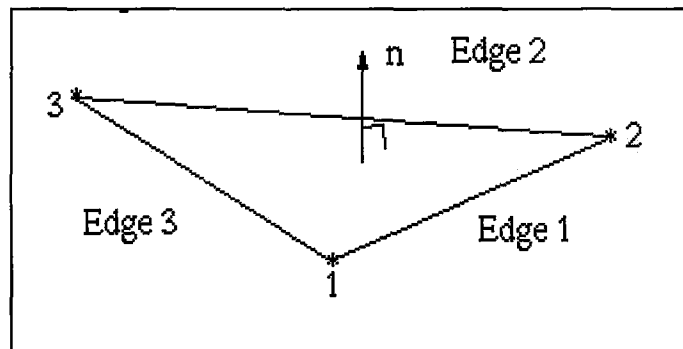


Figure 2.3 A linear triangle thin shell element

2.3.3 Lumped Mass Element

A lumped mass element concentrates mass at a node as given in Figure 2.4. The lumped mass elements are suitable for structural analyses such as normal mode dynamics, linear statics, constraint mode dynamics, linear buckling and nonlinear statics. This type of elements has a topology of one node with three translational degree of freedoms and three rotational degree of freedoms. The translations are in the directions of the nodal displacement coordinate system axes and have the dimensions of length. The rotations are about the nodal displacement coordinate system axes and are measured in radians.

In order to create a lumped mass element on surfaces, edges or curves; the material or the physical properties of the element must be specified. This can be done by using the attributes menu. Then by selecting any points, reference points, centerpoints, vertices or location on edges or surfaces the location of the lumped mass element can be defined. The software creates nodes at those points and

generates geometry-based lumped mass. Then by using the other element types like beam or shell the rest of the solid model can be meshed.

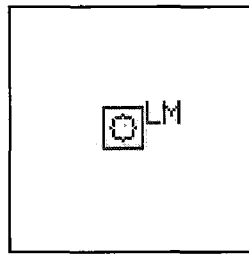


Figure 2.4 The symbol of lumped mass element

2.4 Solid Modeling of the Wing and Components

The solid model of the wing has two main parts, namely the center wing and the outer wing. The center wing has a constant chord without dihedral but the outer wing is tapered with 3° dihedral, has $3^\circ 51' 36''$ sweepback at quarter-chord and an incidence angle of 3° . Each part contains their own skin, ribs, leading and trailing edges, stiffeners and spars. Only the outer wing has aileron but both the center and the outer wings have one flap which are respectively called inboard flap and outboard flap. Since the wing is composed of many parts, the creation of the solid model requires grouping of some structural parts. This further simplifies the model and helps the mesh generation.

2.4.1 Airfoil

To create an airfoil, the data related to airfoil in two dimension (normalized with respect to chord length in x and y directions) must be entered as points by using point creation. In order to get the actual dimensions of the airfoil the center wing chord length is taken as 3000 mm and the chord length for the tip of the outer wing is taken as 1200 mm. Then all normalized coordinates are multiplied with

these values. The previously created points are later joined by using spline operation which is a modeling tool in I-DEAS and the airfoil is obtained. The airfoil used for this study is NACA 65₃-218. Figure 2.5 represents the airfoil.

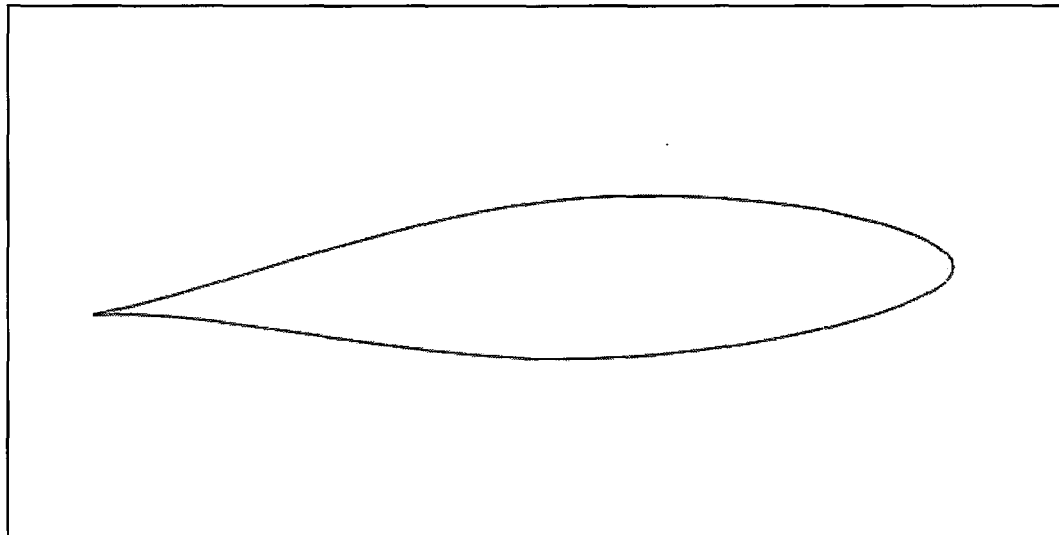


Figure 2.5 NACA 65₃-218 airfoil used for the wing

2.4.2 Skin

The upper and the lower skins are created at the same time by using the loft operation. This operation can be applied across sections, edges or between two existing surfaces. If surfaces over two or more closed sections are lofted, the solid part will be created. If this operation is applied over two or more open sections, then one ends up with a surface. For the wing considered the incidence angle and the dihedral is given to the model by using reference planes which are auxiliary planes used to define the start and end locations of the cross-section used for the loft. After the loft operation, the wing can be considered as a solid part, but deleting any surface from the skin will change the model to zero thickness group of surfaces. More detailed information about the definition of the skin thicknesses will be given in the meshing.

The wing starts from the longitudinal center line of the aircraft and this starting point is assumed as station number zero. The center wing and the outer wing span lengths are 4250 and 8000 mm respectively. Figures 2.6 to 2.8 give the various views of the wing.

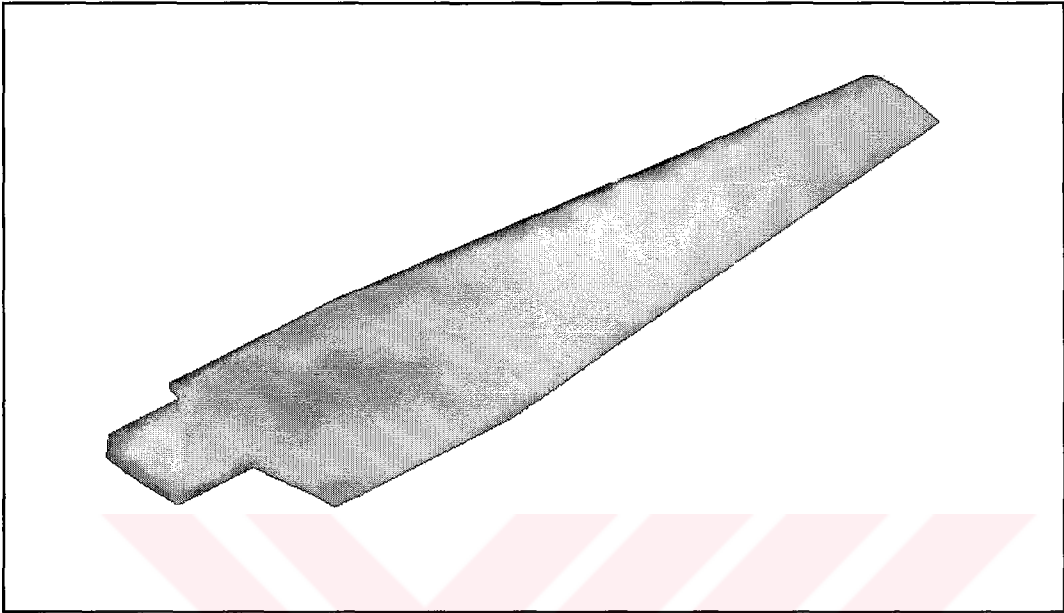


Figure 2.6 Isometric view of the wing

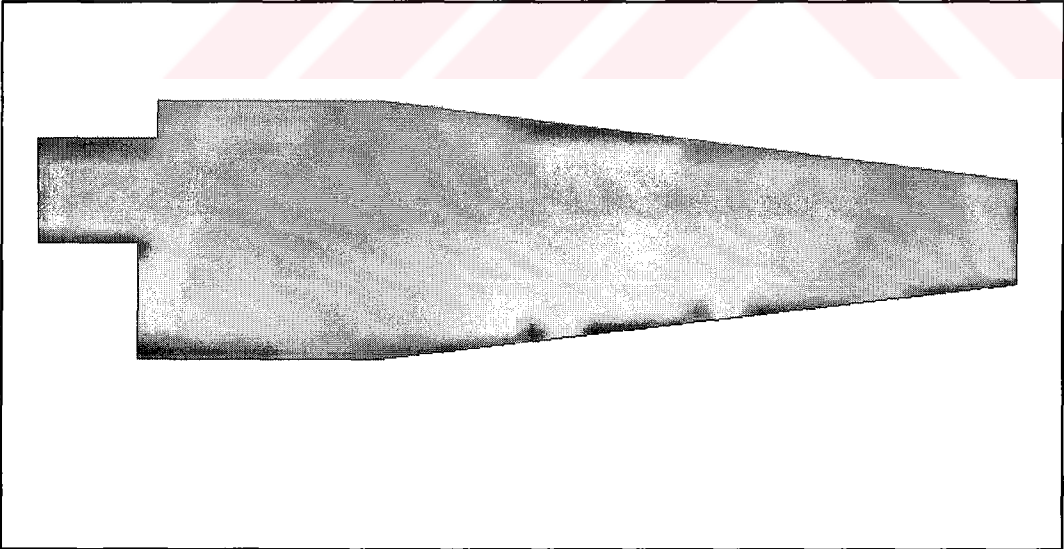


Figure 2.7 Top view of the wing

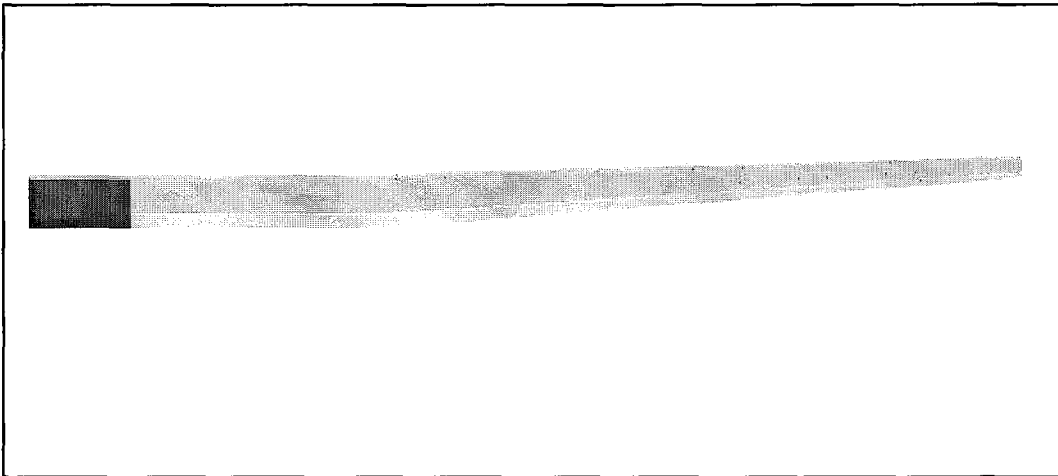


Figure 2.8 Side view of the wing

2.4.3 Ribs

First the locations of the ribs on the wing are determined and the corresponding reference planes are drawn at those locations. These locations are measured in millimeters from the longitudinal center line of the aircraft and identified by station numbers (STA). Two different I-DEAS modeling tools can be used to model the ribs of the wing. One is called the extrude/split surface and the other one is referred to as the loft/split surface. Both extrude/split surface and loft/split surface operations create edges on the surface of the wing. In order to create the surface of the ribs, the surface by boundary operation can be applied to these previously generated edges and with the help of the sketch on place command the necessary modifications such as fillets, holes etc. can be performed. Finally, by applying the surface delete operation to full circles located on the ribs, the holes are created and the general form of the ribs are obtained. The extrude/split surface is used for the center wing having parallel ribs without any incidence and the loft/split surface is used for the ribs of the outer wing with 3° incidence. Figures 2.9 to 2.12 show the wing ribs.

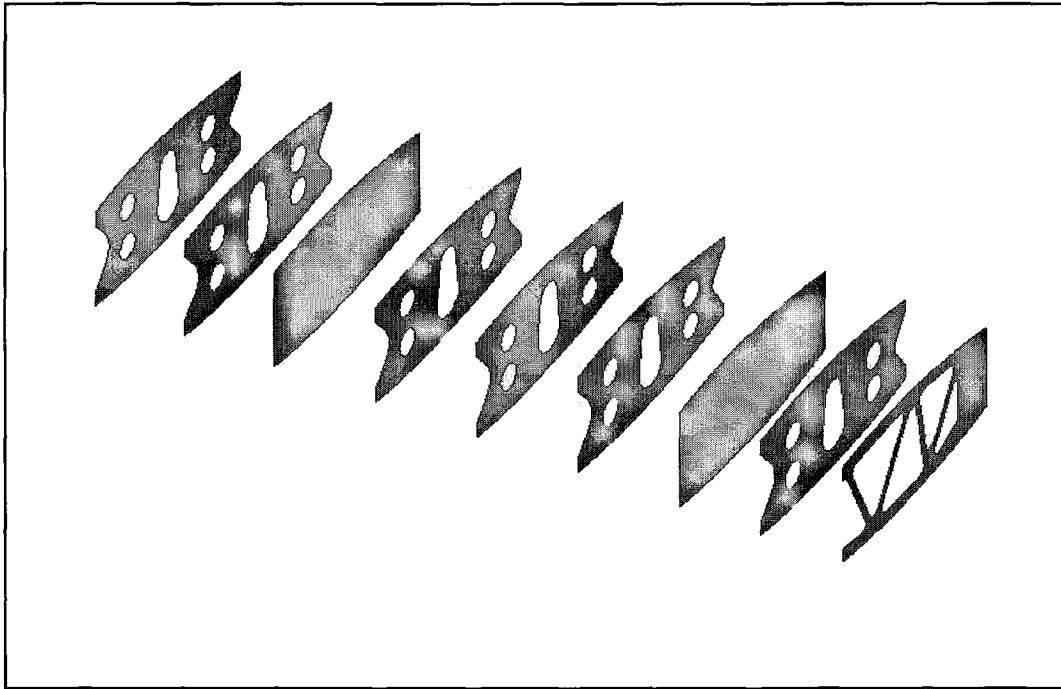


Figure 2.9 Isometric view of the center wing ribs

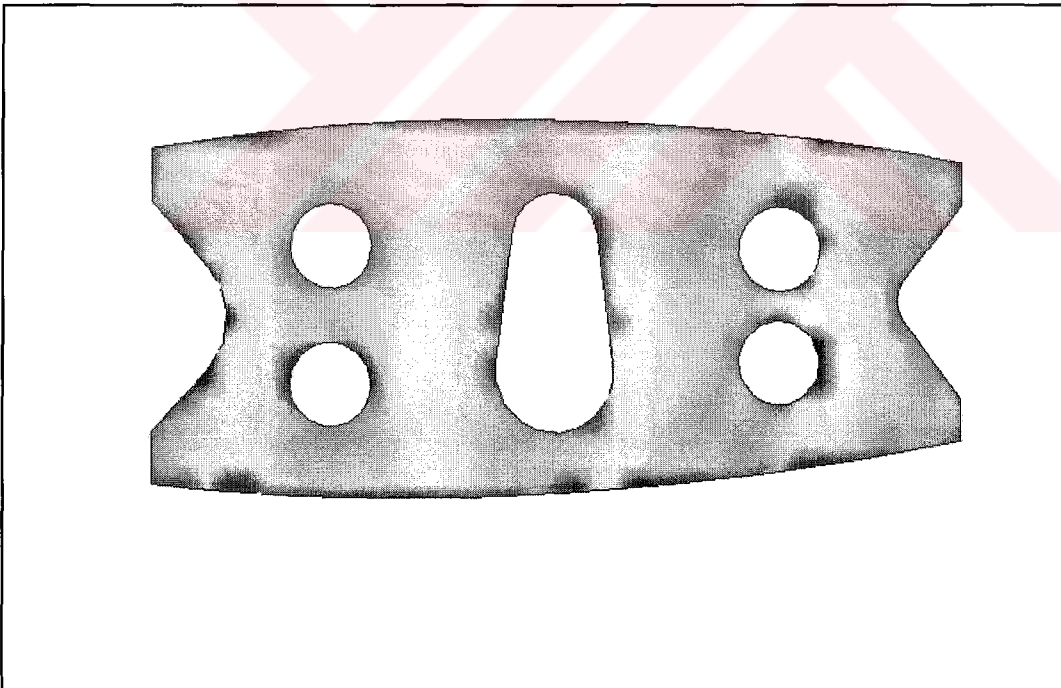


Figure 2.10 View of a rib of the center wing

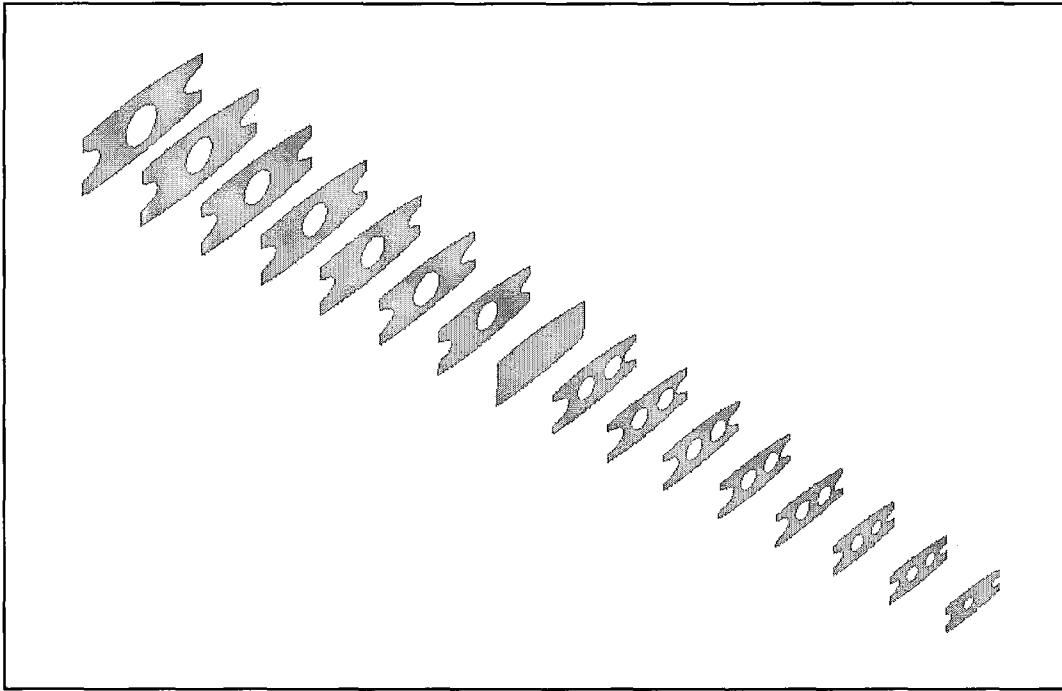


Figure 2.11 Isometric view of the outer wing ribs

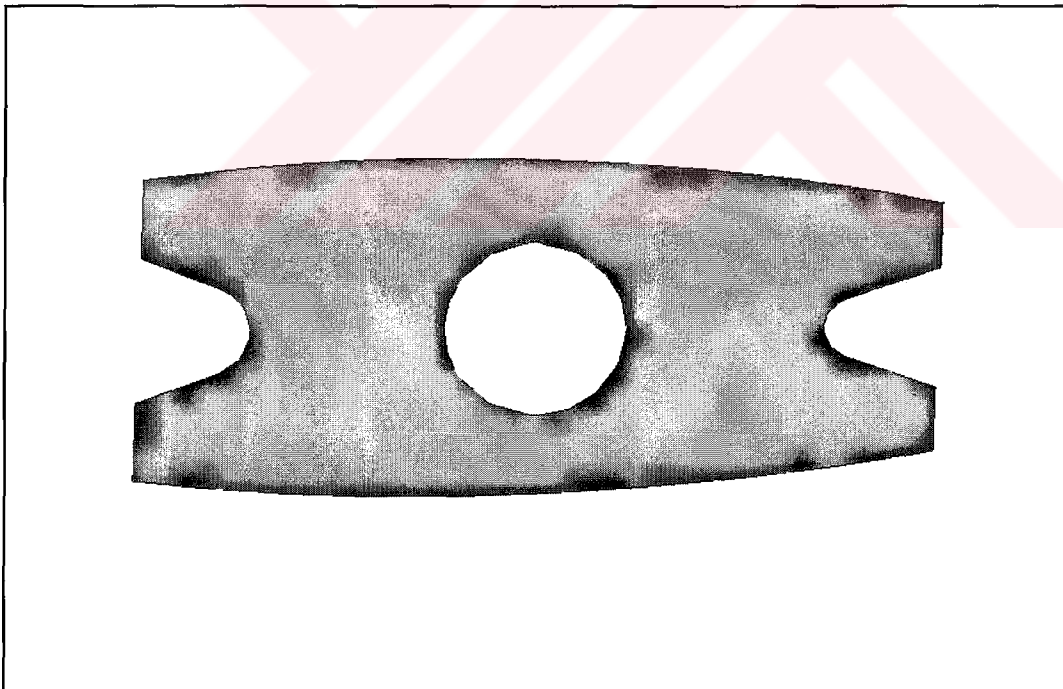


Figure 2.12 View of a rib of the outer wing

2.4.4 Stiffeners

Figure 2.13 shows different stiffener profiles. The stiffeners are located on the upper and the lower surfaces of the center and the outer wing with different profiles in different rib intervals. Therefore, first the starting and end locations in percentage of the chord from the leading edge and the change in profiles between the rib locations are determined. By using the loft/split surface and the project curve on surface operations, the edges belonging to the surfaces of the wing and associated with the stiffeners are created. Those edges are later used to create beam elements on them with real beam geometries.

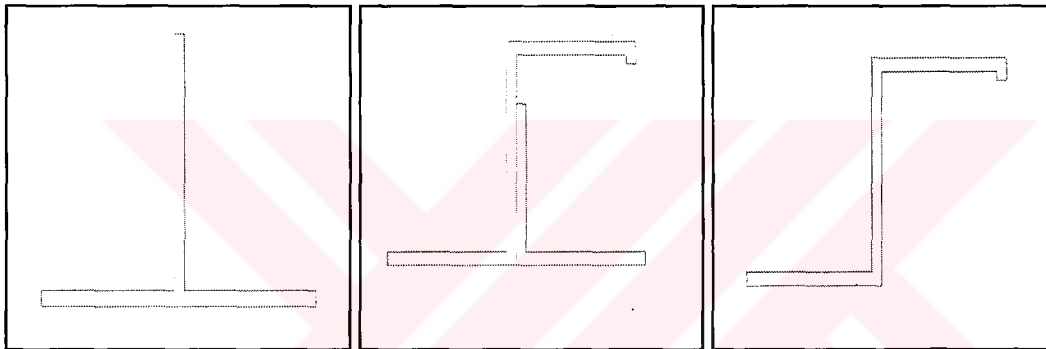


Figure 2.13 Various stiffener profiles

2.4.5 Spars

There are mainly two spars on the wing; front spar and the rear spar as given in Figure 2.14. For the center wing, these two spars are parallel to each other but for the outer wing they are tapered and are not parallel. Each spar is also composed of two parts. One part is the spar web and the other one is the flange of the spar. The same method which is used for the creation of ribs is applied to obtain the spars' web. On the other hand, the creation of beam cross-section, storing the profile, offsetting and orientation of the flange profile procedure should

be followed in order to obtain the flanges of the spar like the profile generation of stiffeners. This procedure will be explained in detail in the meshing.

2.4.6 Leading and Trailing Edges

The leading and the trailing edges of the center and the outer wings are shown in Figures 2.15 to 2.18. They have their own ribs which are connected to the upper and the lower skin of the wing. By using the general rib creation method explained in the ribs section, the ribs of the leading and the trailing edges are drawn and their holes are created. The leading edge has also a small spar in front of the ribs, but trailing edge shares the rear spar of the center and the outer wing.



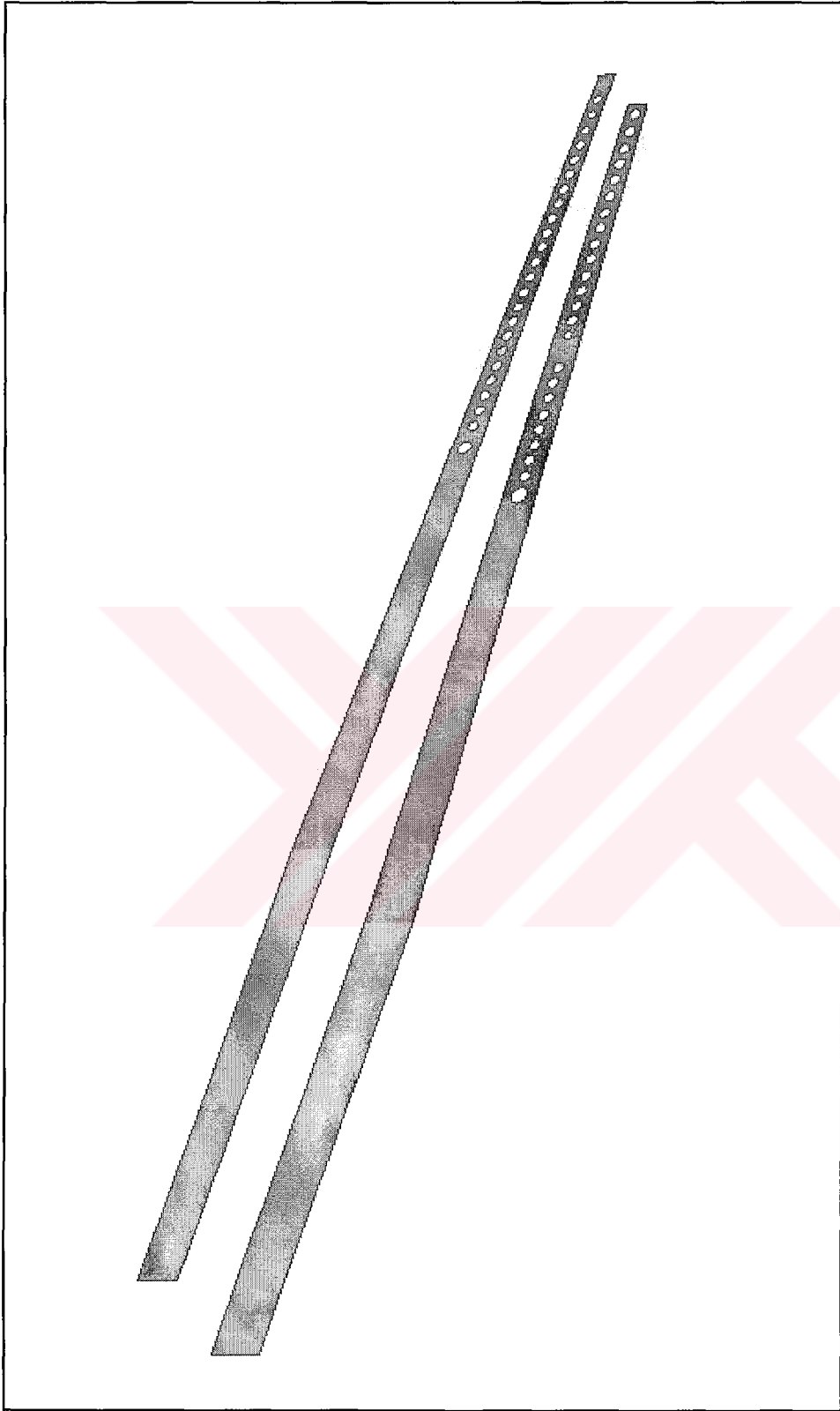


Figure 2.14 Front and rear spar of the wing

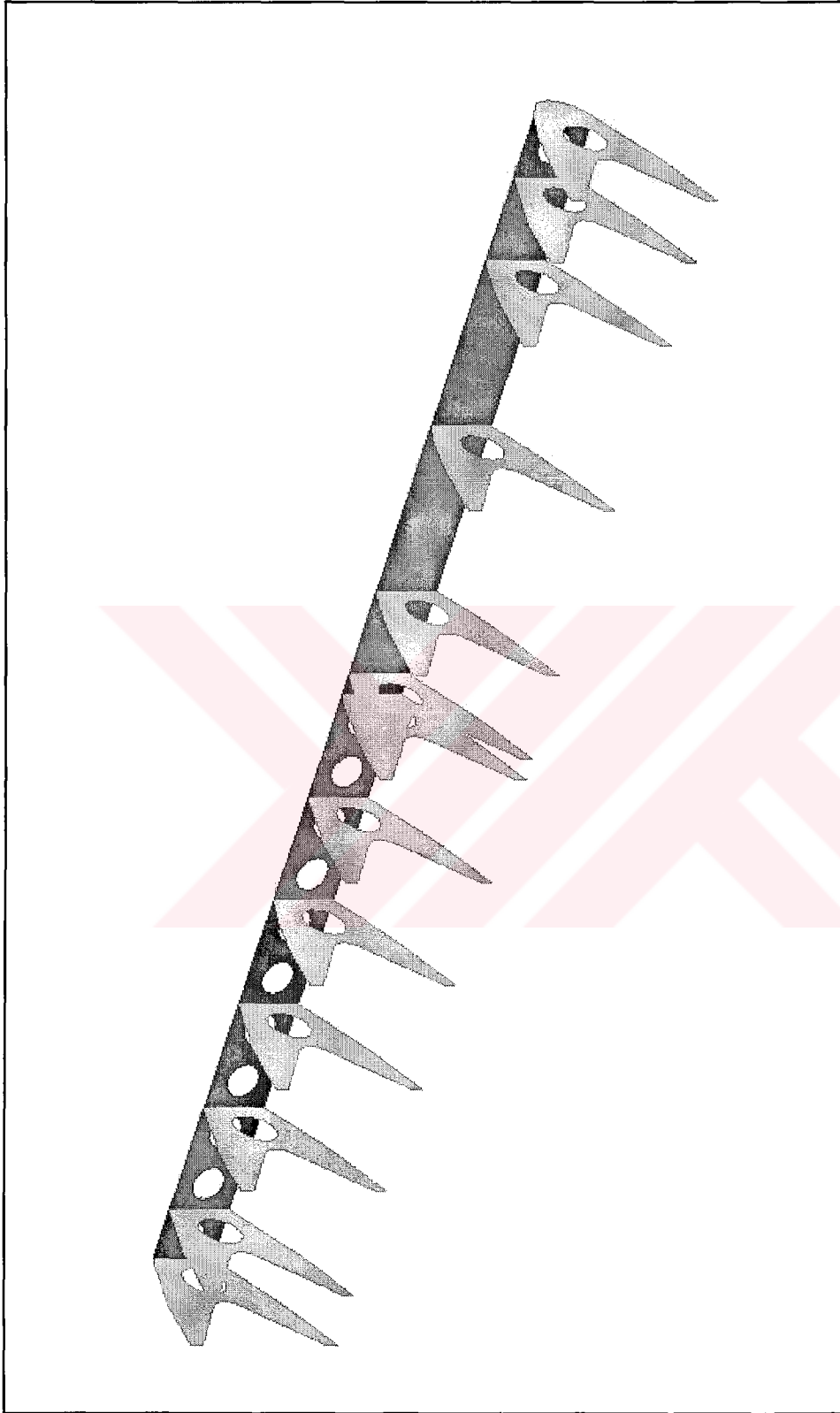


Figure 2.15 Center wing leading edge (ribs and spar)

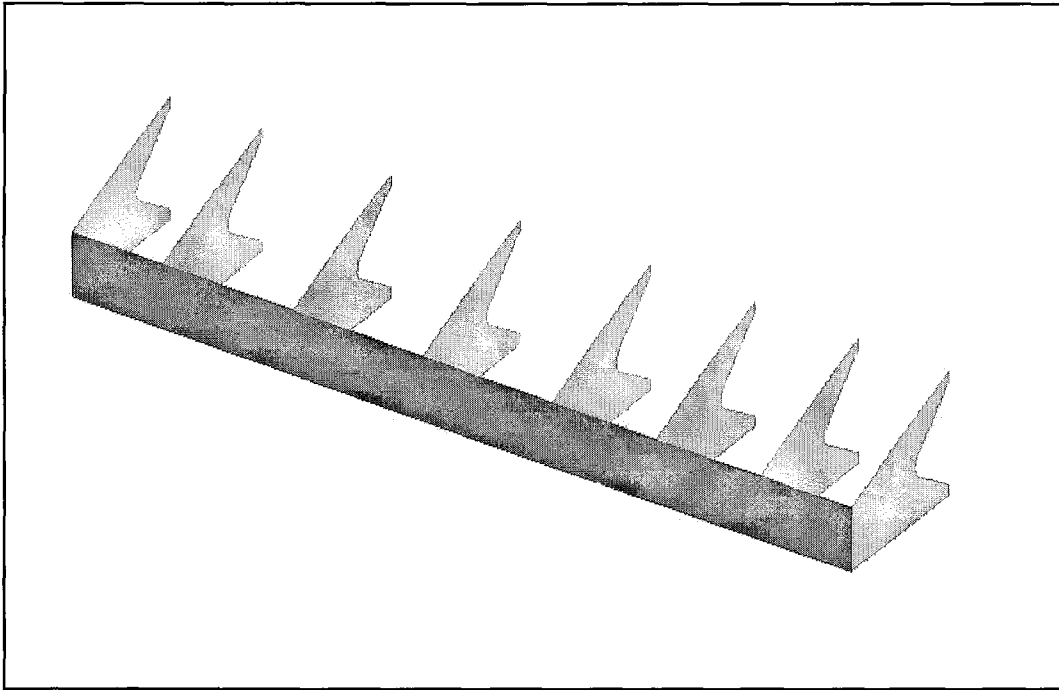
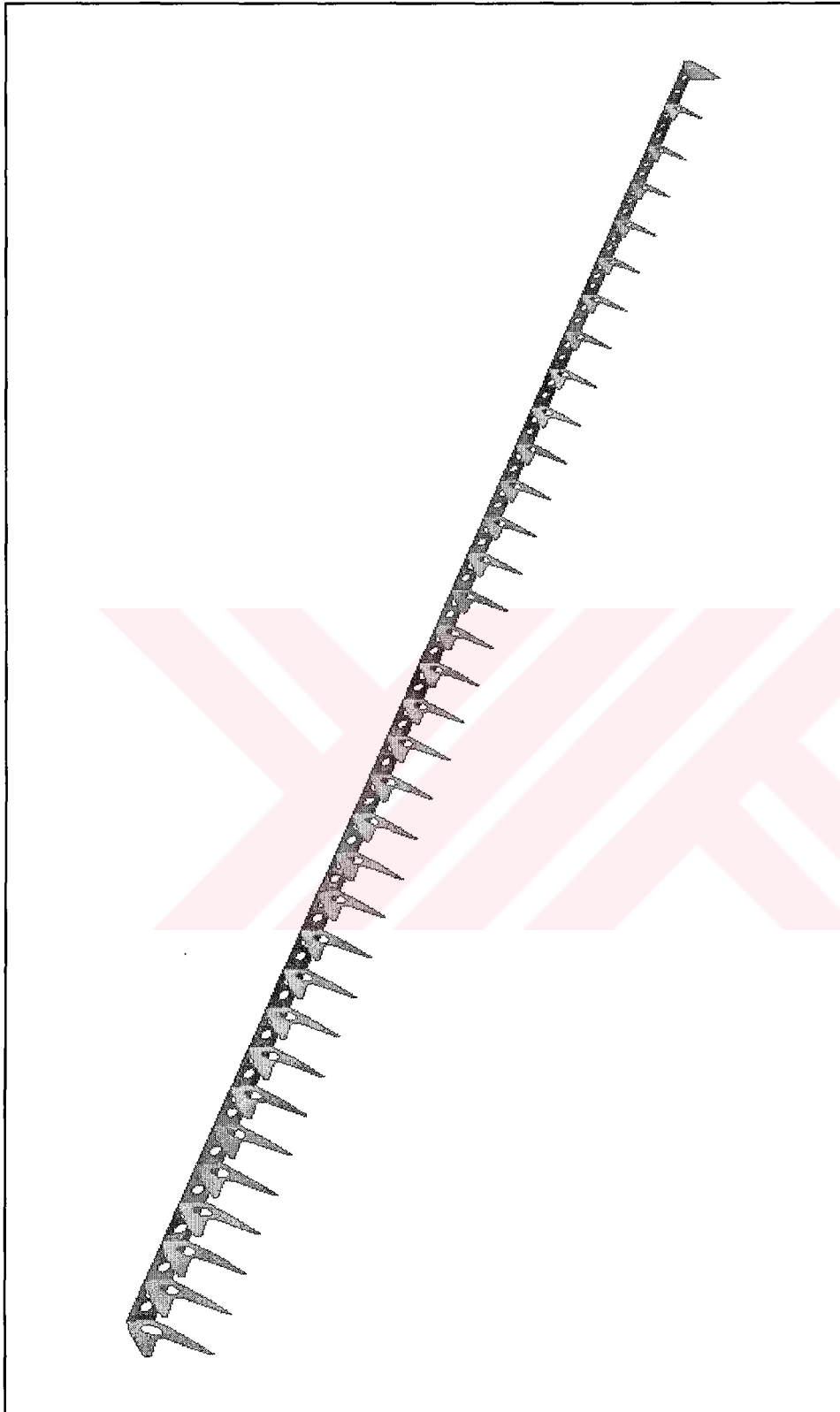


Figure 2.16 Center wing trailing edge

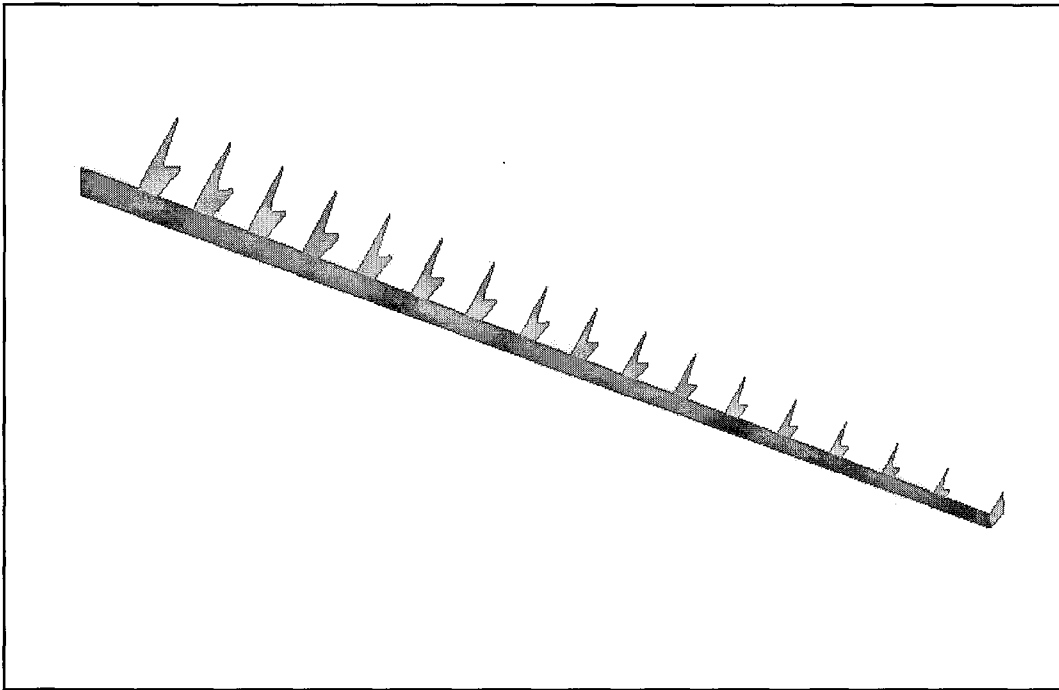
2.4.7 Flap and Aileron

These two control surfaces have their own spar and ribs. When modeling the spar of the flaps, which are illustrated in Figure 2.19 and 2.20, the flanges are also considered as separate beam parts and their profiles are created. The only difference between the flanges of the main spars (the front and the rear spar of the center and the outer wing) and the flanges of the flap is the thickness and the base length of the beam profiles. In the case of aileron, only the web of the spar is taken into account and the flanges of the spar are neglected since they are very small. Figure 2.21 gives the model of the aileron.

The solid model of the whole wing and all the structural components are shown in Figure 2.22.



2.17 Outer wing leading edge (ribs and spar)



2.18 Outer wing trailing edge (ribs and spar)

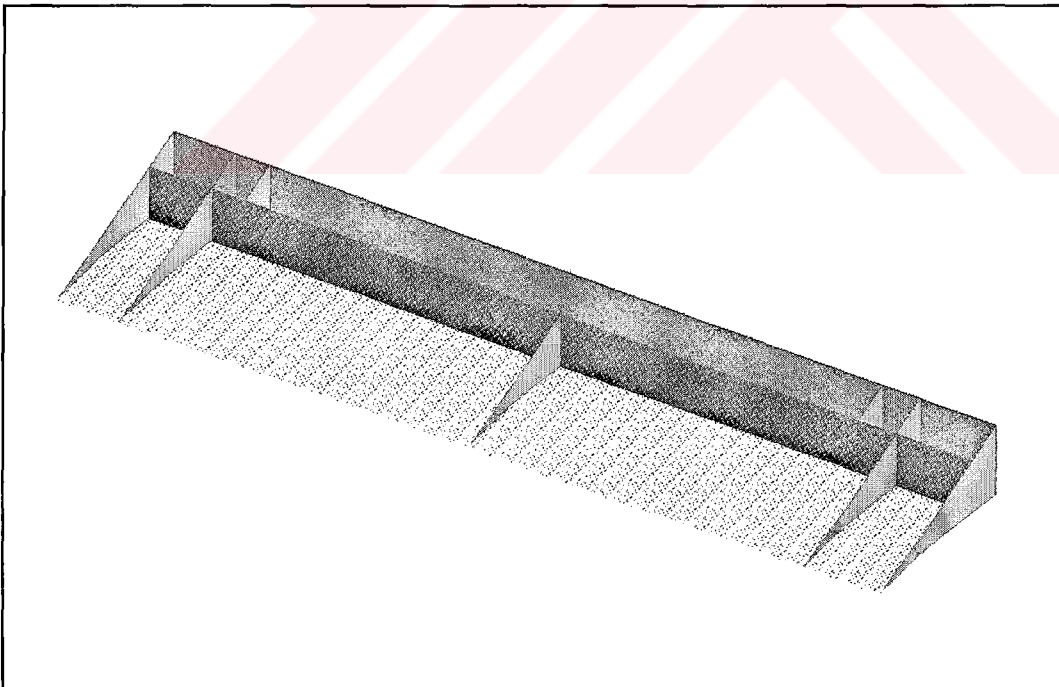


Figure 2.19 Center wing flap (inboard flap)

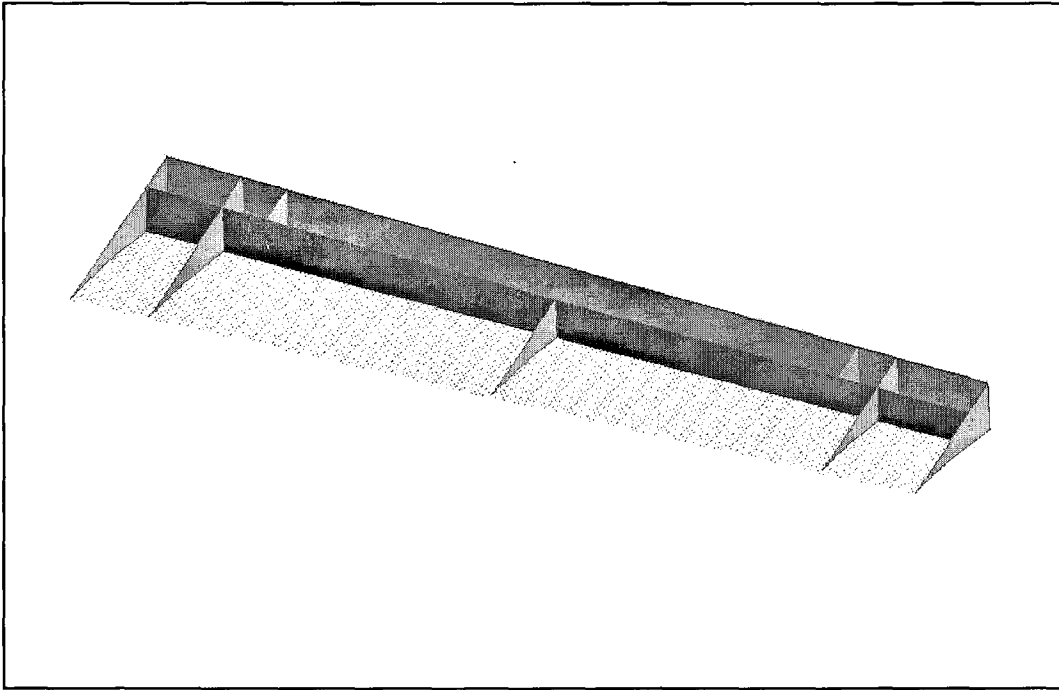


Figure 2.20 Outer wing flap (outboard flap)

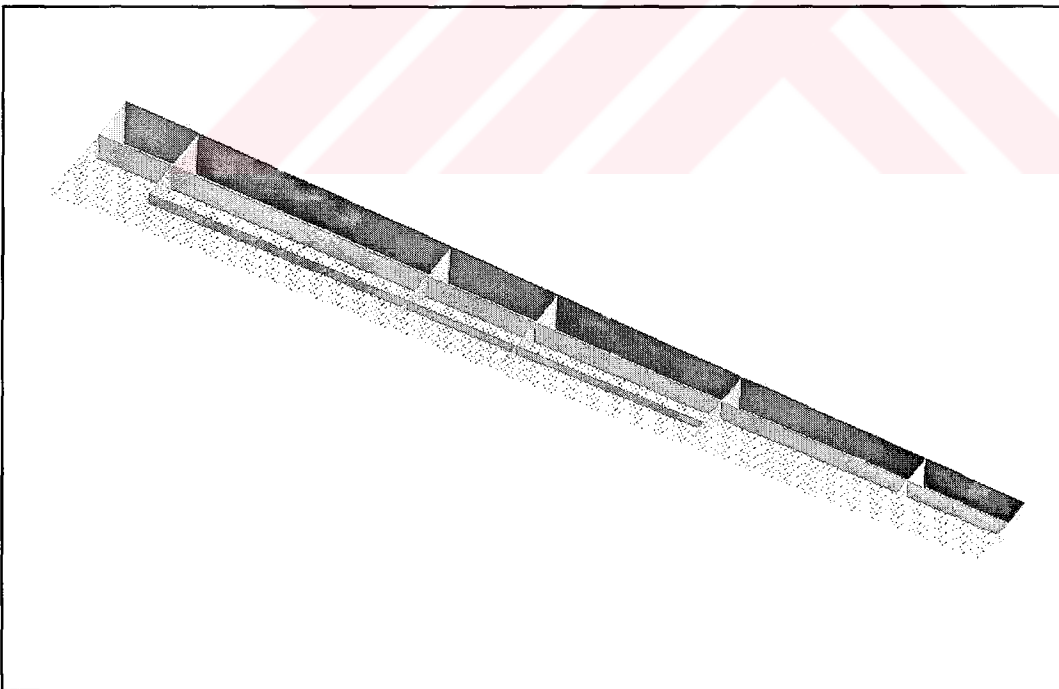


Figure 2.21 Aileron

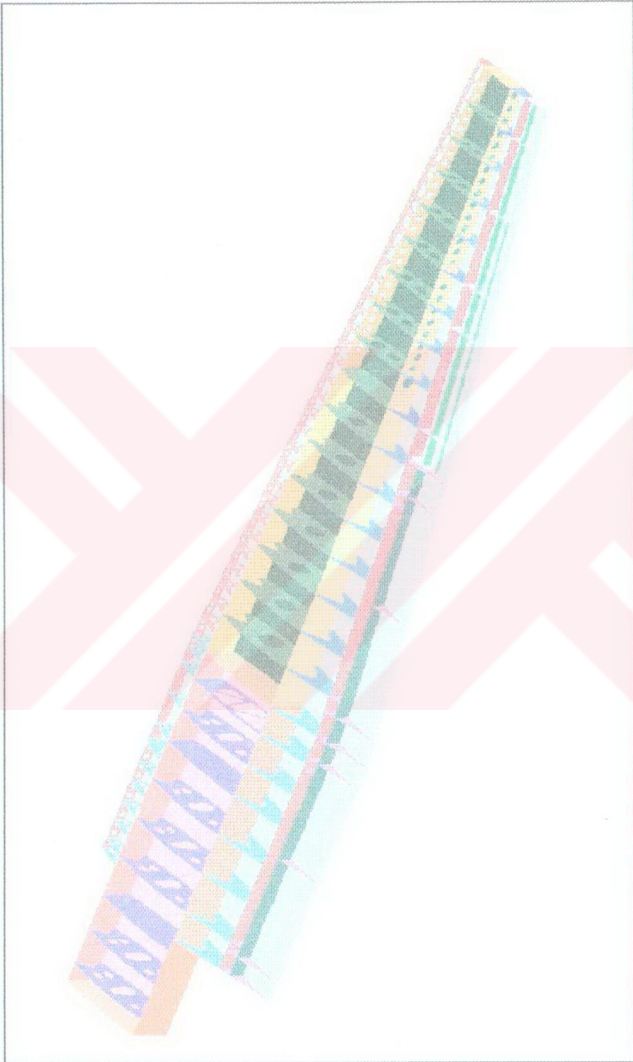


Figure 2.22 Isometric view of the whole wing and structural components

CHAPTER 3

MESHING OF THE WING MODEL

3.1 Introduction

This chapter explains the meshing of the wing model by using the beam, shell and lumped mass elements.

One of the most important and time-consuming steps of a finite element analysis is the meshing of the model. Since the solid model of the wing is obtained in such a way that it was a group of zero thickness surfaces, the thickness information of all structural parts are given to the model during the meshing operation. Therefore, before starting to mesh the model the thickness, physical and material properties of all the structural parts of the wing such as stiffeners, ribs, wing skin, aileron, flaps are obtained.

The best way of creating a mesh is to create the part's geometry and then generate a mesh on the geometry. In I-DEAS, a mesh is related with the geometric entities. Since the finite element model is associated with the part, any change to the part automatically affects the nodes and elements of the mesh [5].

There are two main entities used for the meshing of the wing model, one is the edges and the other is the surfaces. The edges can be used to model the

stiffeners and the flanges of the spars. On the other hand all surfaces belonging to the model are used to mesh the wing skin, the center and outer wing ribs, the front and the rear spar webs, flaps and aileron surfaces, the leading and trailing edges' surfaces and their spars and the ribs. Since those surfaces and edges include different geometrical and thickness information, the meshing may turn out to be a very complex operation. Therefore, in order to solve this complexity and get a fine mesh, the starting point is the grouping of the finite element entities like in the solid modeling part. This time, the group contains the nodes and the elements associated with the edges and the surfaces of the wing solid model.

In the meshing operation, either mapped or free meshing can be selected. Mapped mesh is a regular mesh on surfaces, sections or volumes and it is impossible to create a mapped mesh on curves or edges. Mapped meshing requires that a surface or section has three or four sides and should not contain any holes. On the other hand free meshing automatically generates nodes and elements on surface and solid geometry and allows more flexibility than the mapped mesh since the boundaries of the surfaces and the volumes can be more complex. Free meshing can mesh surfaces including holes (in the solid model of the wing, these correspond to the center and outer wing ribs and the front and rear spar webs of the outer wing) and volumes including holes and interior voids. Additionally, the free mesh generator uses an algorithm that tries to minimize element distortion which is a very important parameter from the point of view of accuracy of the solution. Therefore, because of the complexity of the model and due to the advantages the free meshing operation is selected in this study.

3.2 Meshing with Different Elements

In the study the structural parts of the wing solid model are meshed by using different types of elements. The beam and shell elements are mainly used and wherever necessary the most suitable element type is selected for the meshing of the wing geometry.

3.2.1 Structural Parts Meshed by Beam Elements

The upper and the lower stiffeners and the flanges of the front, rear and flap spars are modeled by using one dimensional linear beam elements. A very long procedure is followed during the beam element meshing.

First the profile of the stiffeners and the flanges are determined and then by using beam section tool of I-DEAS, the beam geometries are defined. The beam section tool enables one to create beam cross-sections either by using standard sections or general beam cross-sections from a wireframe geometry. The former is an easy and quick way to generate rectangular cross-sections used for the flanges of the front, rear and flap spars and also for the upper and lower stiffeners of the center wing and the inner part of the outer wing. The latter uses a wireframe geometry that was created in the Master Modeler module of I-DEAS. By using the drawing tools of the Master Modeler the wireframe geometries are obtained and the sections are created (refer to Figure 2.13). Then the geometry of the wireframe section is transferred to the general beam section. In order to do this the beam cross-section must be stored. Before storing the general cross-section the cross-section's properties are evaluated.

Each element in the finite element model must have a physical property table. This table lists each physical property for an element and the numerical value for each property. For beam elements the cross-sectional area, perimeter, principal I_y and I_z , eccentricity in Y and Z directions, offset rotation angle are considered as physical properties. Before meshing, the physical and material properties and the element length of the beam are also defined and the edges associated with stiffeners or flanges are determined and selected.

The stiffeners and the flanges of the spars are modeled by using the edges. The beam options form of I-DEAS allows one to get a beam cross-section and define the elements along the edges. These edges are located in three-dimensional space by making an angle with the global coordinate system. Additionally the

beam cross-section has principal axes which are not coincident with the global axes of the model. Since the stiffeners are tangent to the surface of the wing and the flanges of the spars are located not only tangent to the surface of the wing but also directed into torque-box of the wing, both beam cross-sections for the stiffeners and the flanges must be oriented.

If the wireframe geometries of beam cross-sections are selected for the meshing operation, the geometrical properties of the cross-section are calculated by I-DEAS with automatically generated surface mesh. Then the principal axes of the cross-section are also determined and shown on the section. Figure 3.1 represents a mesh and calculated principal axes for a beam section. Symbol ‘ * ’ defines the shear center and the points denoted by 1 to 5 are the stress points which are automatically created by I-DEAS. The bending, axial and shear stresses are evaluated at each point and from these stress components Von Mises stress can be found. After the calculations of necessary properties, all the values related with the cross-section are stored by using the beam store option.

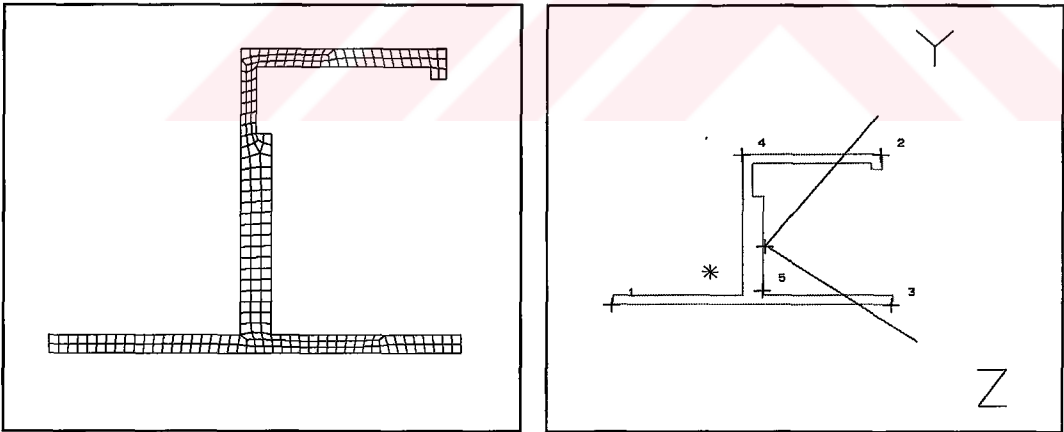


Figure 3.1 The mesh and the calculated principal axes for a beam section

The orientation procedure is relatively simpler for the rectangular beam cross-sections since all the geometrical properties of the cross-section are automatically calculated by I-DEAS without generating any mesh over the surface of the beam cross-section. The orientation can be given to beam element by changing the orientation angle of the cross-section about the beam axis which matches with the selected edge for the meshing.

Different beam cross-sections are used to mesh different parts of the wing. The upper and the lower stiffeners of the center wing are meshed by rectangular cross-sections given in Figure 3.2 and the other types of cross-sections are used for meshing the outer wing stiffeners. Figure 3.3 represents the stiffeners used in the outer wing.

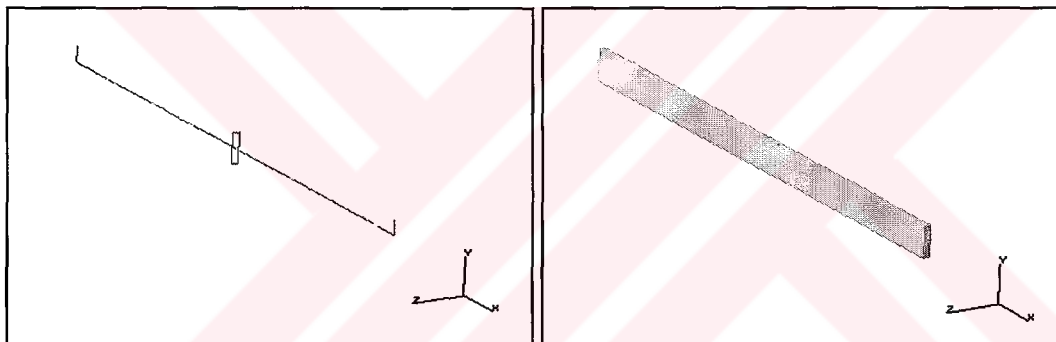


Figure 3.2 Beam element used as a stiffener for the center wing
and the solid view of the element

The location and the profile of the stiffeners also change from one station to another. Figures 3.4 and 3.5 show the upper stiffener locations on the center and the outer wing skin respectively.

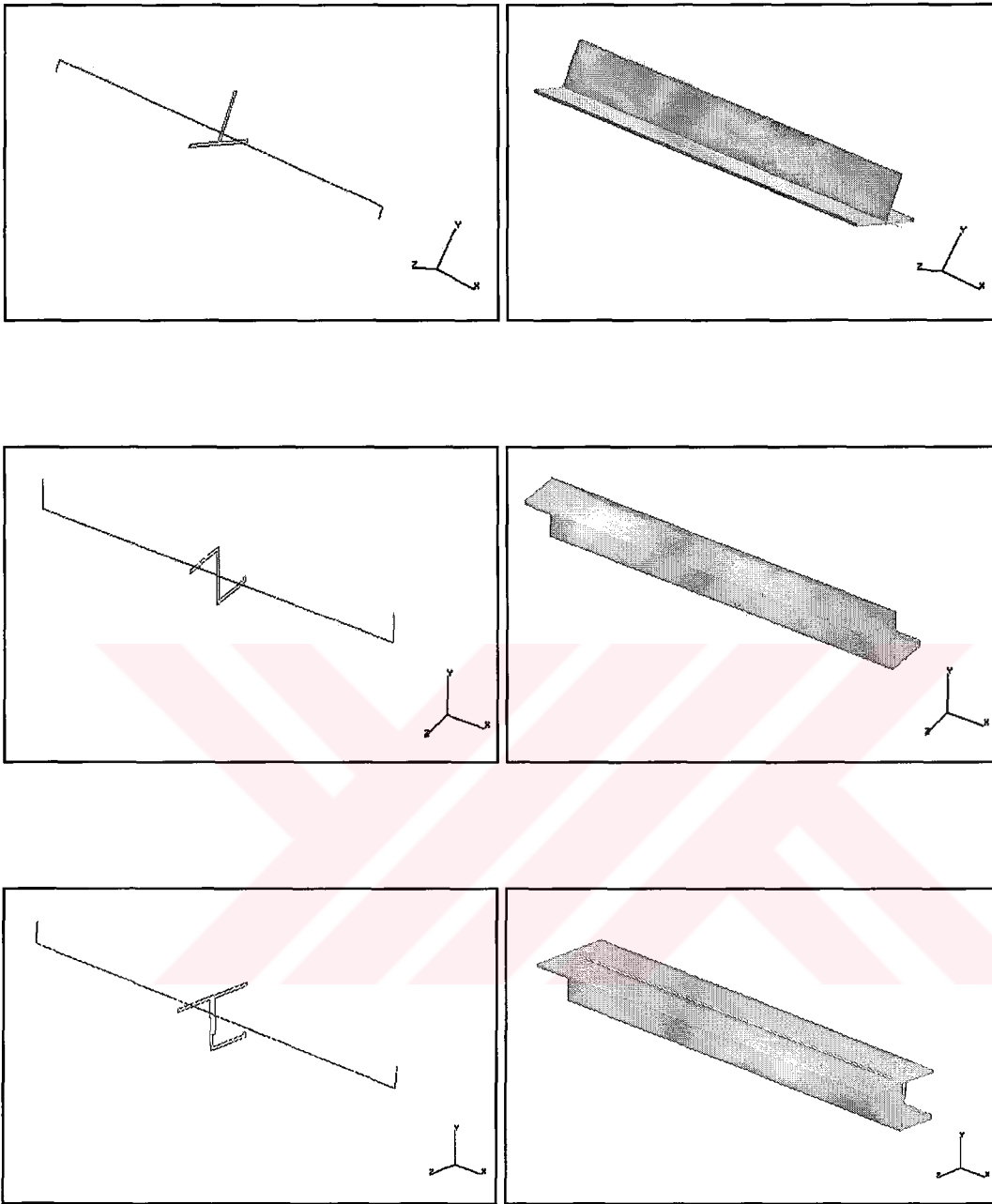


Figure 3.3 Beam elements used as stiffeners for the outer wing
and the solid view of the elements

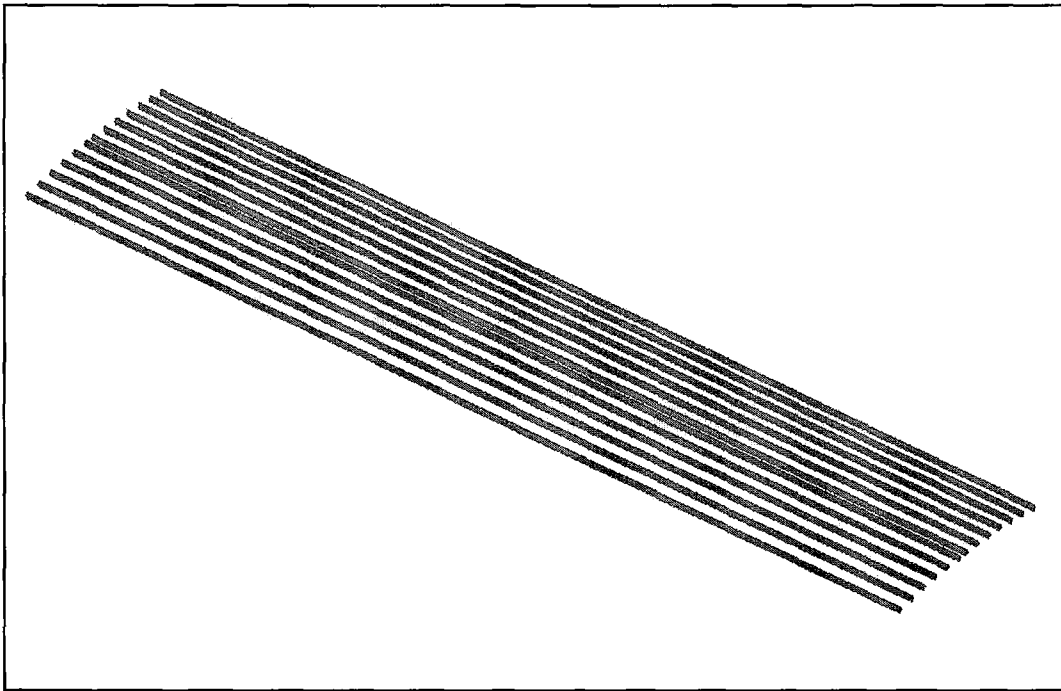


Figure 3.4 Locations of the center wing upper stiffeners

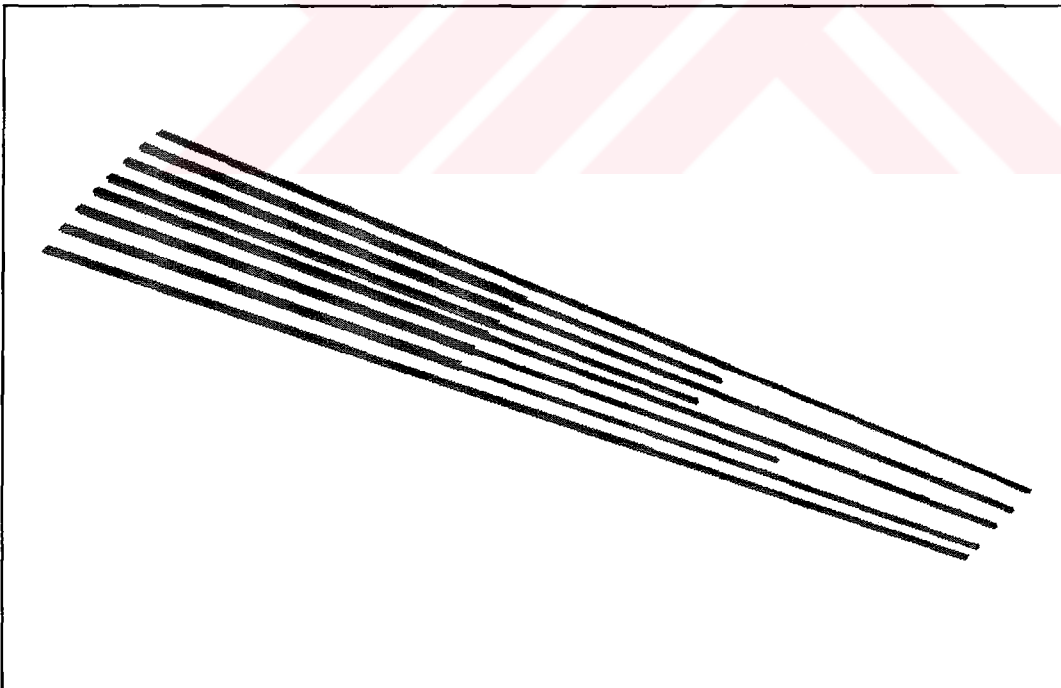


Figure 3.5 Locations of the outer wing upper stiffeners

The meshing of the flanges of the center and the outer wing spars are done by using another rectangular cross-section. This time the offset is very important since the offset distance given in Y and Z directions directly affects the stiffener type. For example, the offset distance given to element in Z direction changes the spar geometry from I-beam to C-beam. Figure 3.6 represents the case that the offset distance is given to beam element in Z direction.

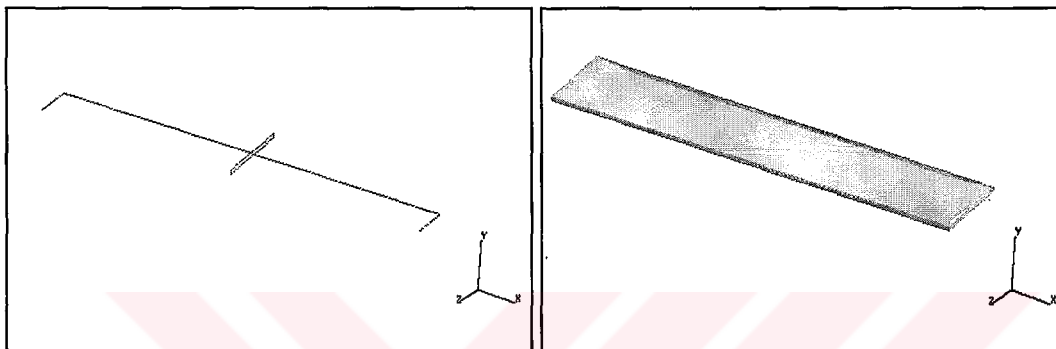


Figure 3.6 Beam element used as a flange for the center and outer wing spar and solid view of the element

All these operations simulate a condition that a beam is welded onto the surface of a part and this is the real situation for the stiffeners and flanges located under the wing skin. This case is shown in Figure 3.7.

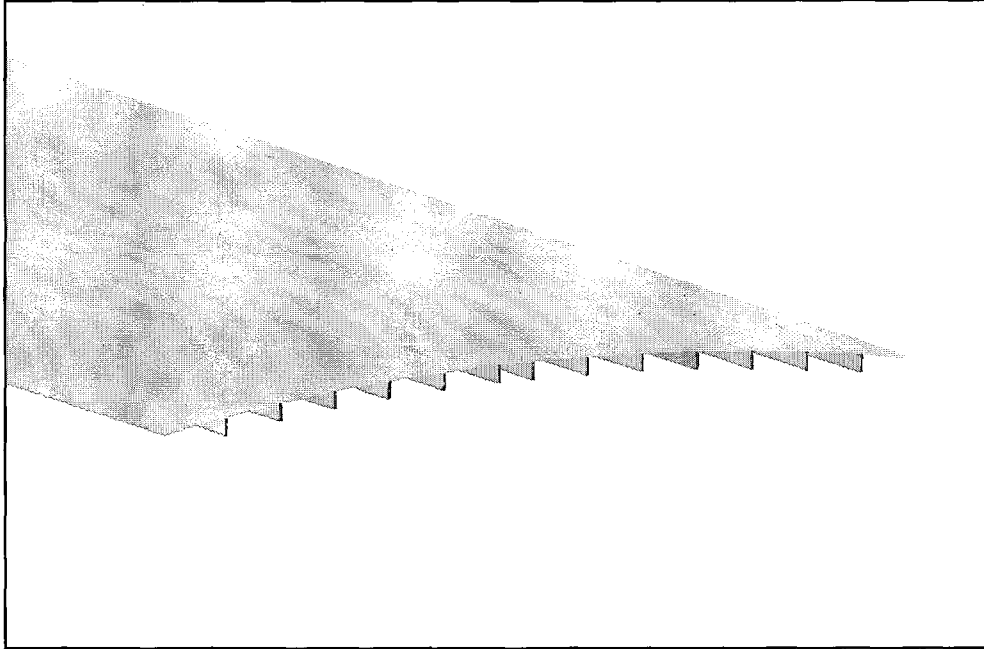


Figure 3.7 The orientation of the stiffeners under the skin of the center wing

3.2.2. Structural Parts Meshed by Shell Elements

All surfaces of the wing are modeled by using the shell elements. These surfaces include whole the upper and the lower skin of the wing, ribs of the center and the outer wing, front and rear spar web surfaces, leading and trailing edge spar web and rib surfaces and finally flaps and aileron surfaces.

In the model, since all the surfaces have different thickness values, the shell elements having these thicknesses must be defined before starting to mesh the corresponding surfaces. In order to obtain the elements with material and thickness information the physical property tool of I-DEAS is used. In the thickness definition part, I-DEAS asks the thickness value for each node of the element. Entering the same thickness to all nodes creates an element having a uniform thickness throughout the nodes. Then, this element can be stored with a special name. After defining all the elements, that will be used in the model, with different

names and corresponding thicknesses the structural parts of the wing are ready to mesh.

For the meshing of the surfaces either linear quadrilateral thin shell element with four nodes or linear triangle thin shell element with three nodes can be used. In the analysis the structural parts having small holes or surfaces having curved edges are meshed by using the triangle elements. This type of elements are also preferred to get a finer mesh with smaller element length and less number of nodes as compared to the quadrilateral elements.

The following step is the selection of the surfaces to be meshed. By suitably determining the element type and the element length, all the surfaces of the wing skin and the structural parts can be meshed.

In some cases, the determination of the element length can be a quite difficult task. For example the surface can be bounded by its periphery with the neighborhood elements or nodes. In this case, the mesh does not depend on the element length specified and causes a very coarse mesh. The solution to these type of problems is to define an anchor node which is a finite element entity attached to the geometry. The advantage of using an anchor node is to force a node at its location during free mesh generation. Anchor nodes are related to geometry and are history-supported. That is, if the geometry changes, the anchor nodes are updated on the revised geometry at the appropriate locations. Therefore, the nodes created at the locations of the anchor nodes during the free mesh generation will also be updated on the revised geometry. During the meshing of the wing the anchor nodes are used to obtain a finer mesh for small surfaces with curved edges of the wing such as the leading edge ribs. Symbol ‘*’ stands for the anchor node and Figure 3.8 shows the leading edge rib meshed by using the anchor nodes.

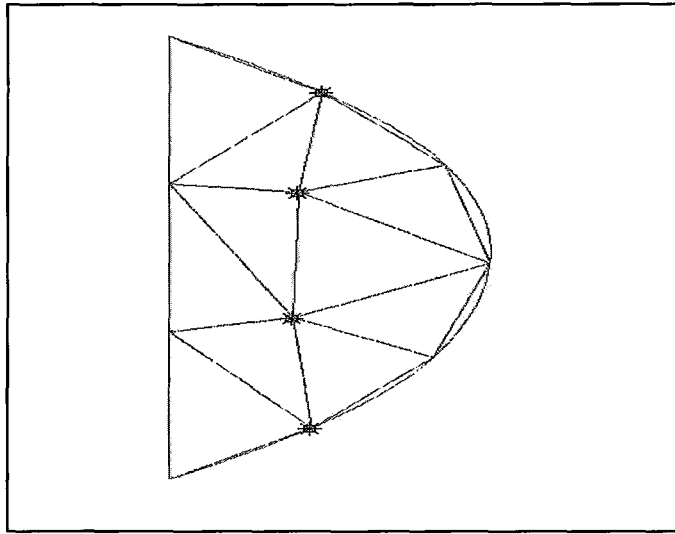


Figure 3.8 Mesh of the leading edge rib and the anchor nodes

Figure 3.9 and 3.10 give the meshed upper and lower skin of the center wing, whereas Figure 3.11 and 3.12 represent those of the outer wing.

Although the most of the center and the outer wing ribs contain holes they are still meshed with quadrilateral elements as shown in Figures 3.13 to 3.16. Since these elements can be used to mesh the large surfaces with less number of the elements, they help to reduce the solution time by controlling the node and the element numbers. By using the same element type the center wing front and rear spar webs are also meshed. On the other hand, some part of the outer wing front and rear spar webs containing many small holes are meshed with the triangle shell elements and Figure 3.17 highlights those. Same meshing technique is also used for the leading edge skin, ribs and spars shown in Figures 3.18 and 3.19 . Similarly the flaps and the aileron trailing edges are meshed and are shown in Figure 3.20. Finally, Figure 3.21 shows the solid view of the mesh of the center wing torque-box with stiffeners.

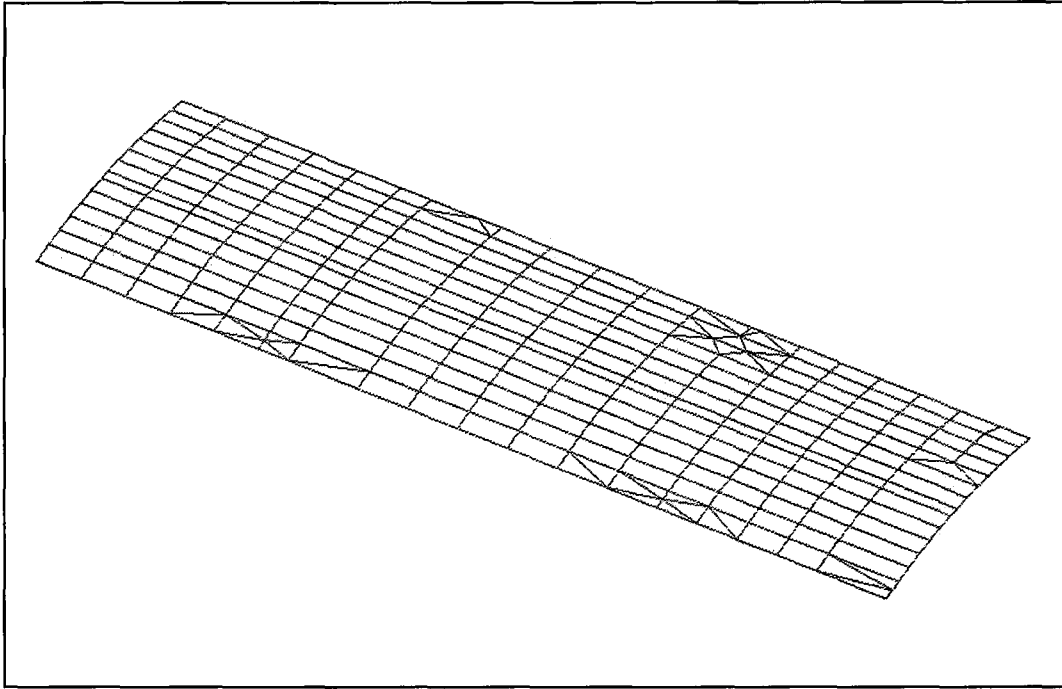


Figure 3.9 Mesh of the upper skin of the center wing

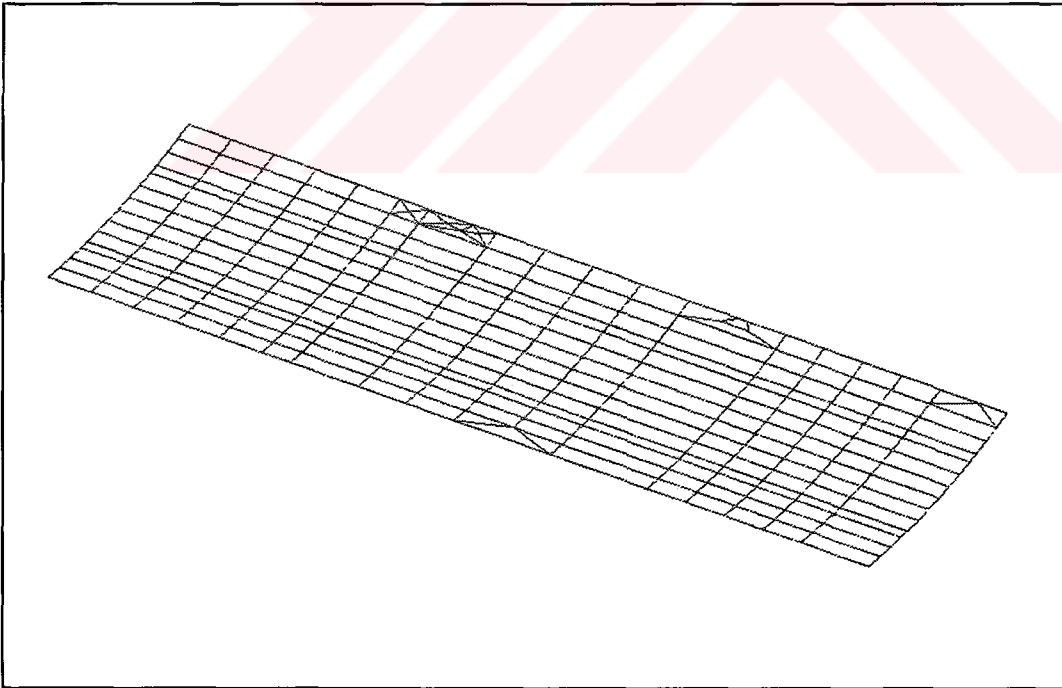


Figure 3.10 Mesh of the lower skin of the center wing

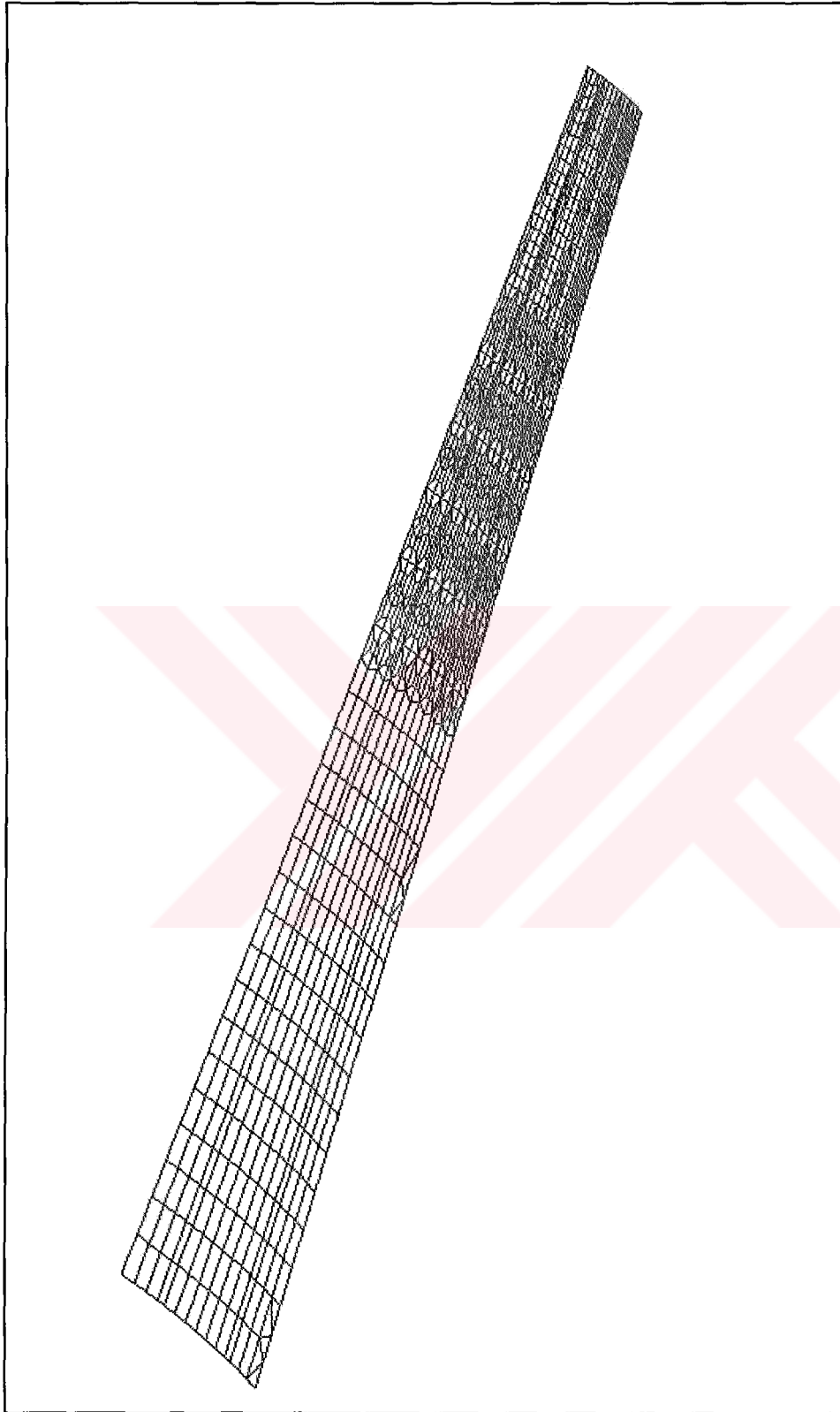


Figure 3.11 Mesh of the lower skin of the outer wing

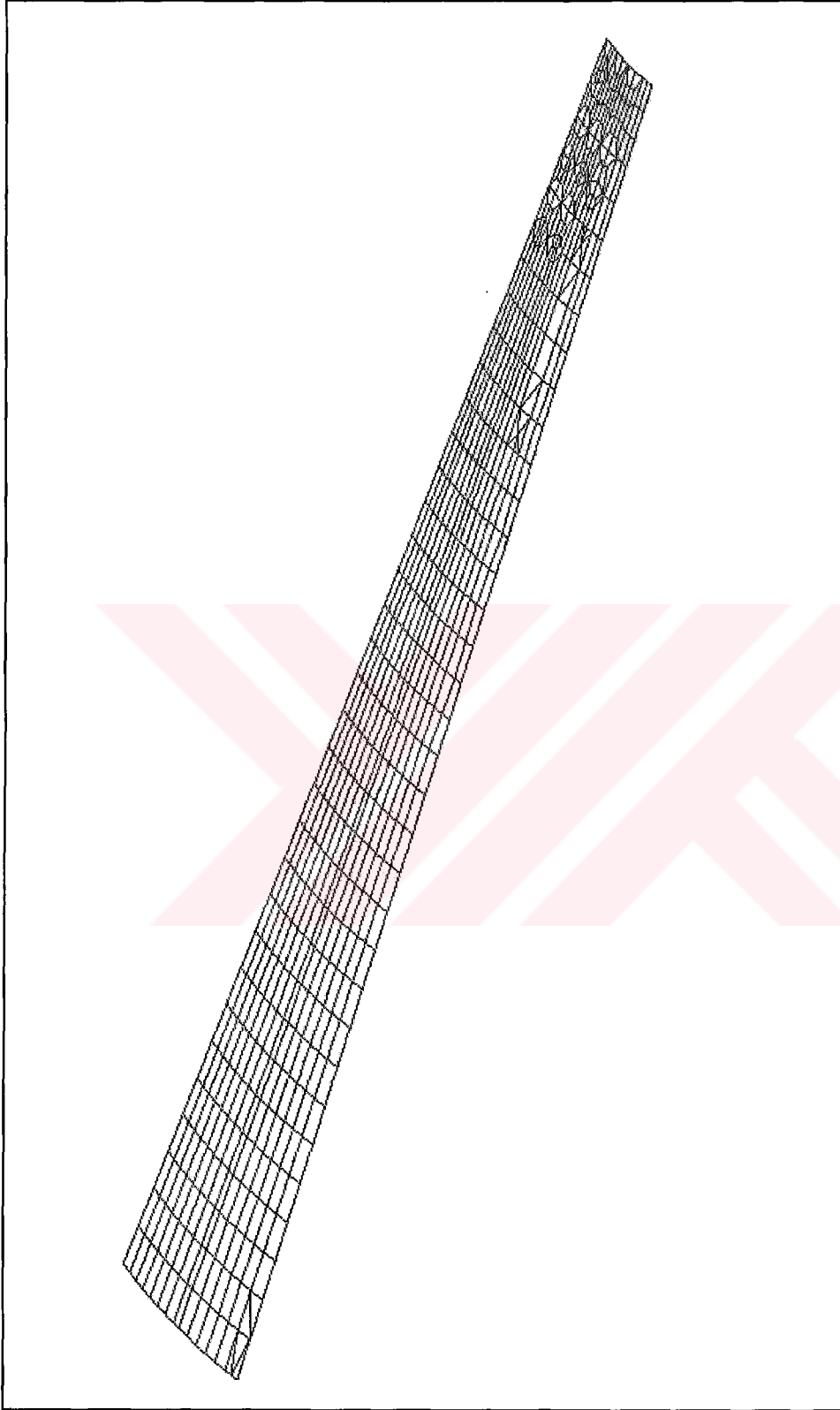


Figure 3.12 Mesh of the upper skin of the outer wing

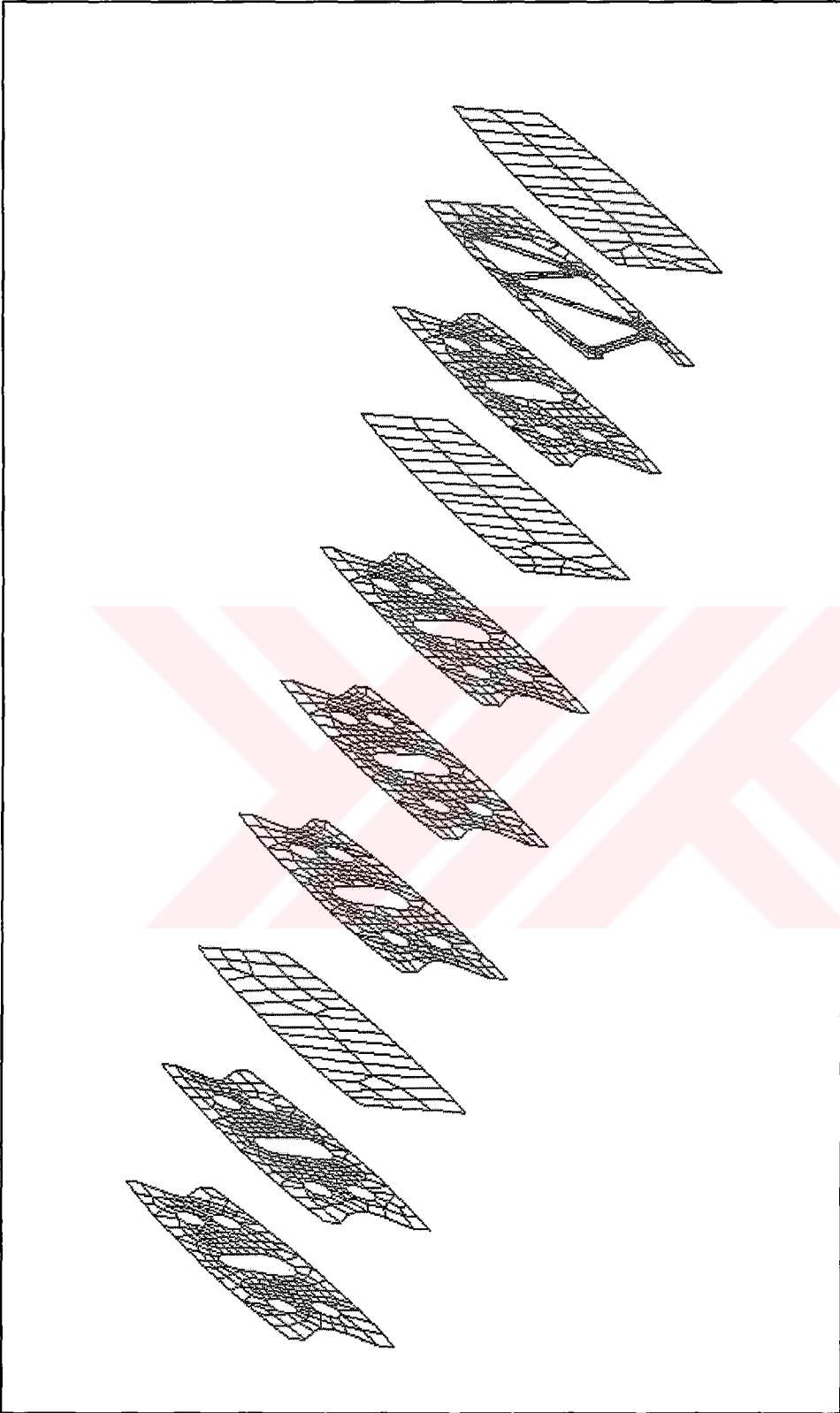


Figure 3.13 Isometric view of the center wing ribs with meshing

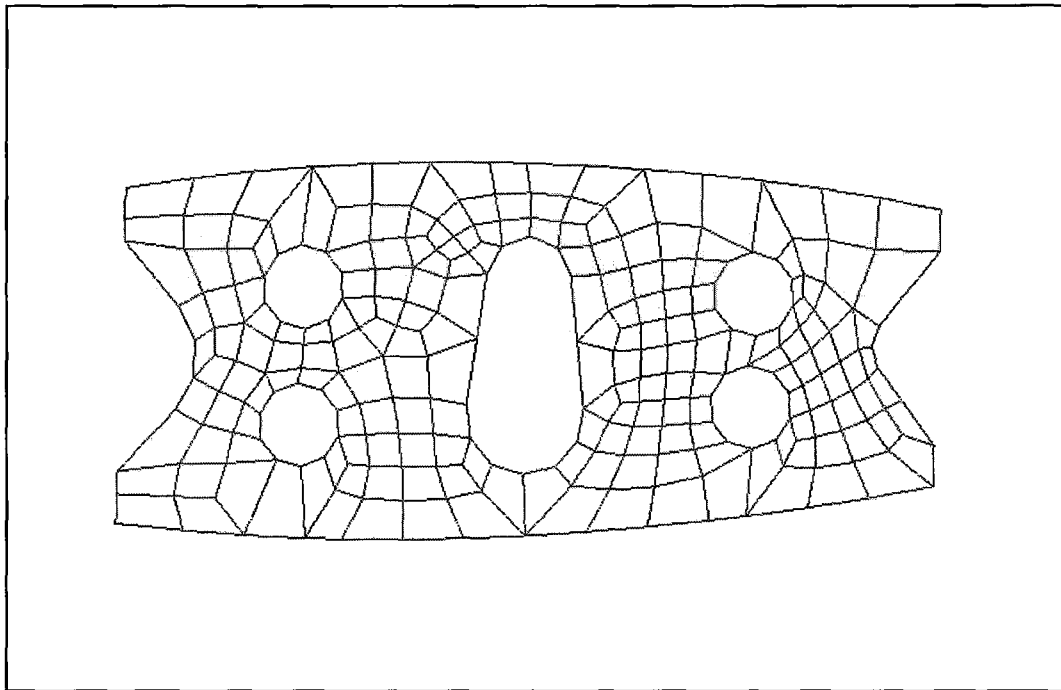


Figure 3.14 A view of a rib of the center wing with meshing

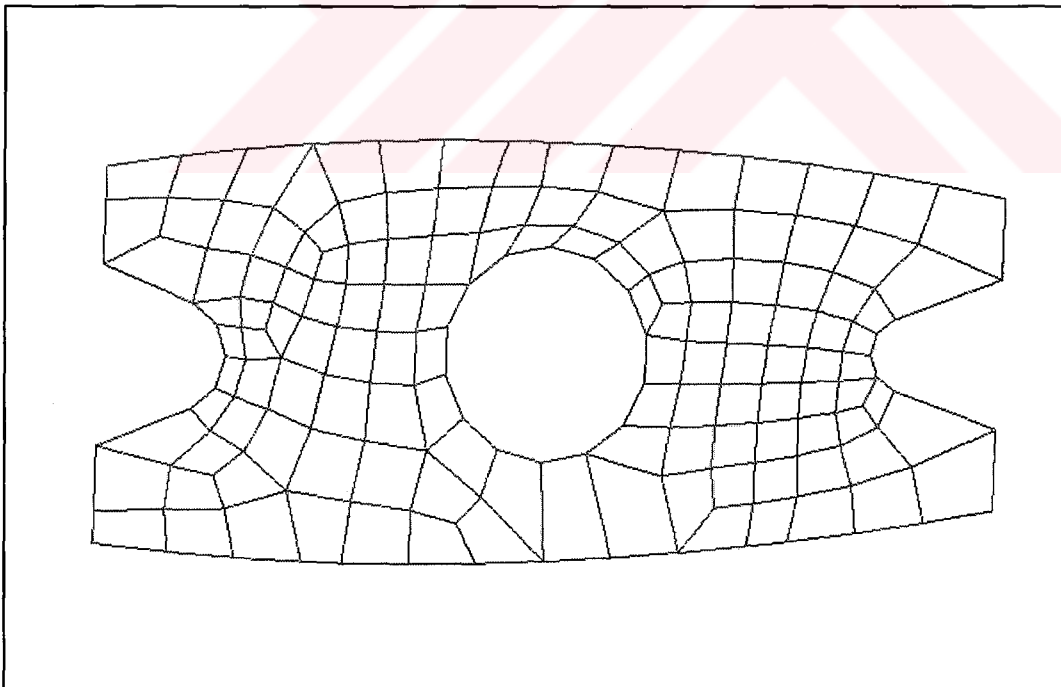


Figure 3.15 A view of a rib of the outer wing with meshing

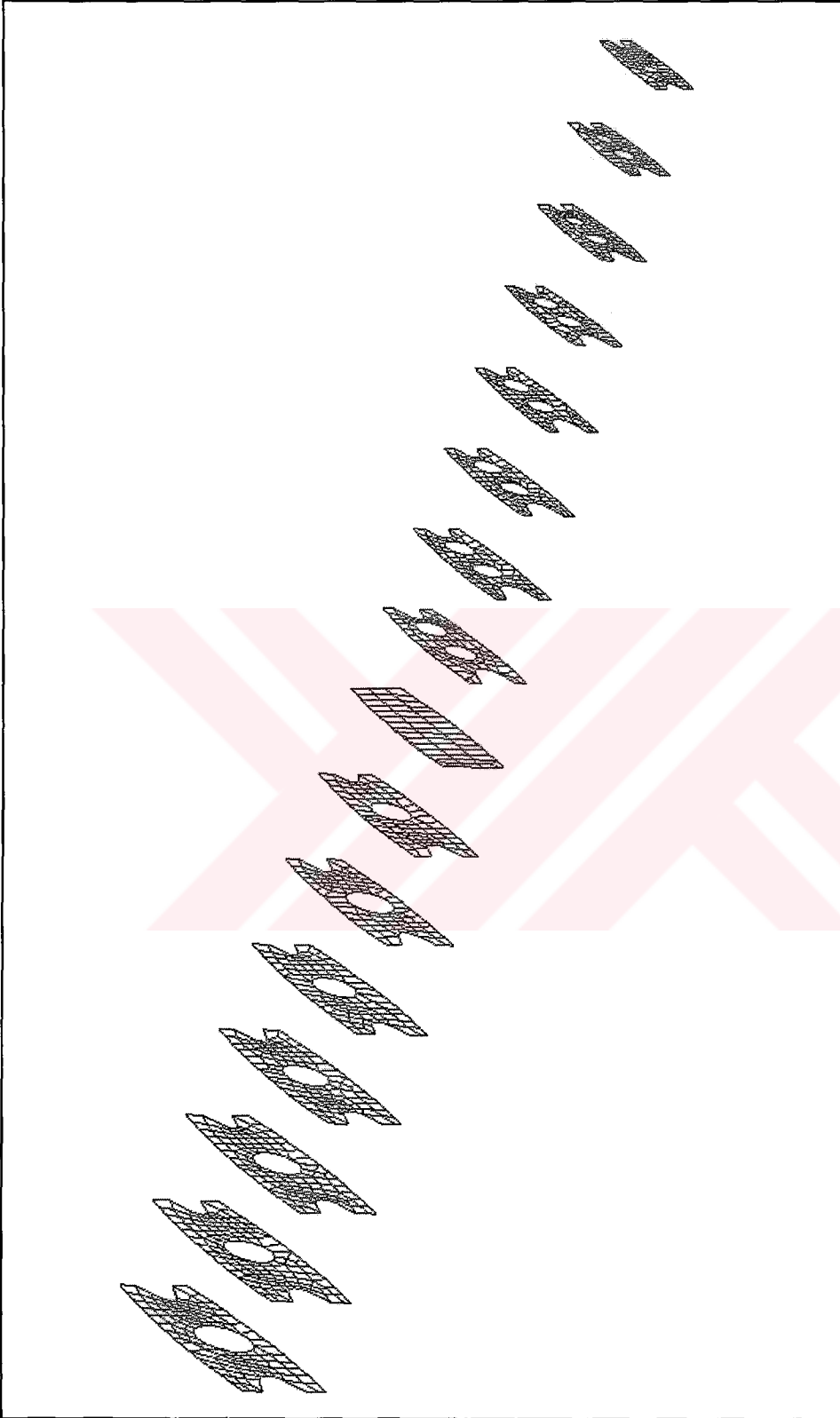


Figure 3.16 Isometric view of the outer wing ribs with meshing

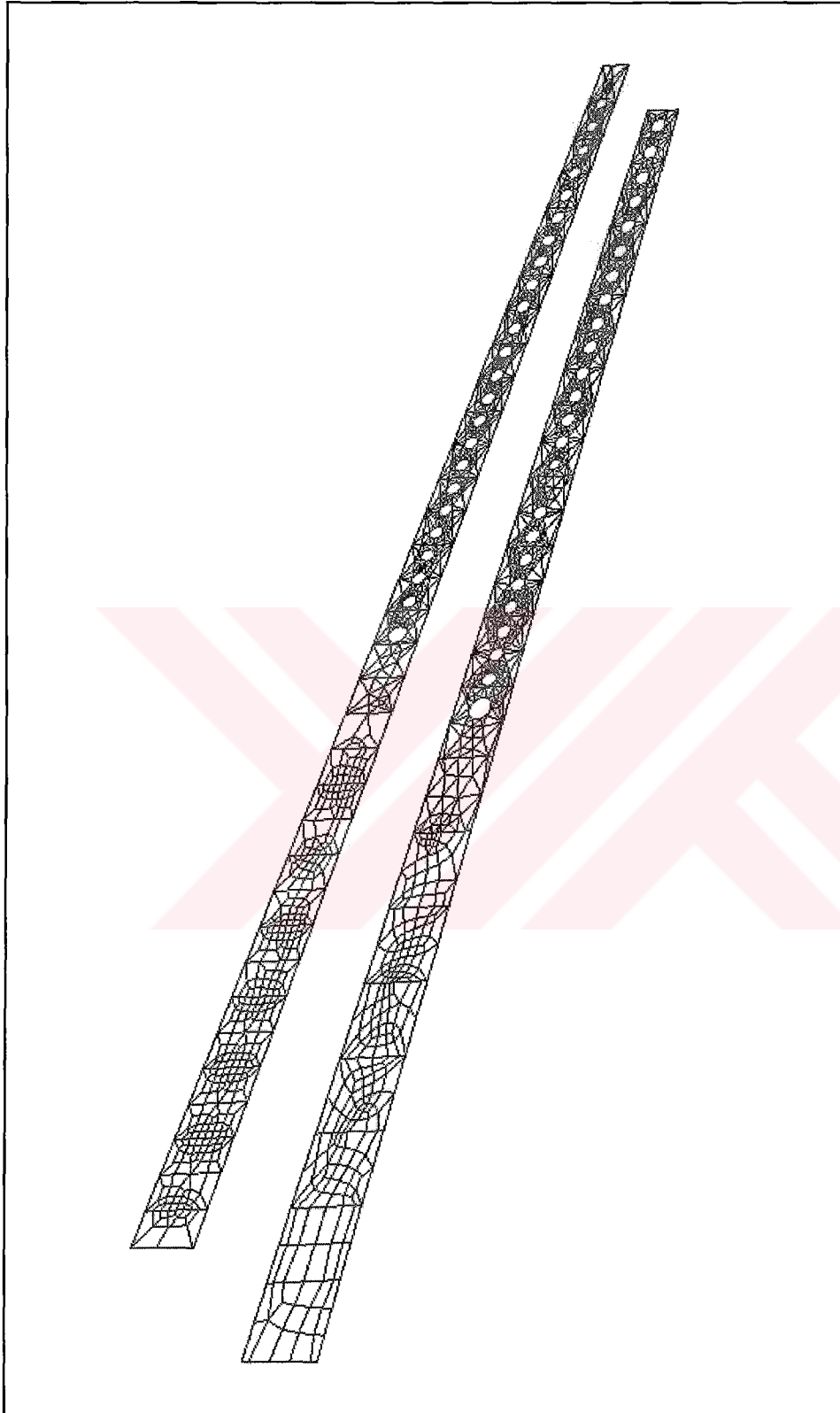


Figure 3.17 Mesh of the outer wing front and rear spars

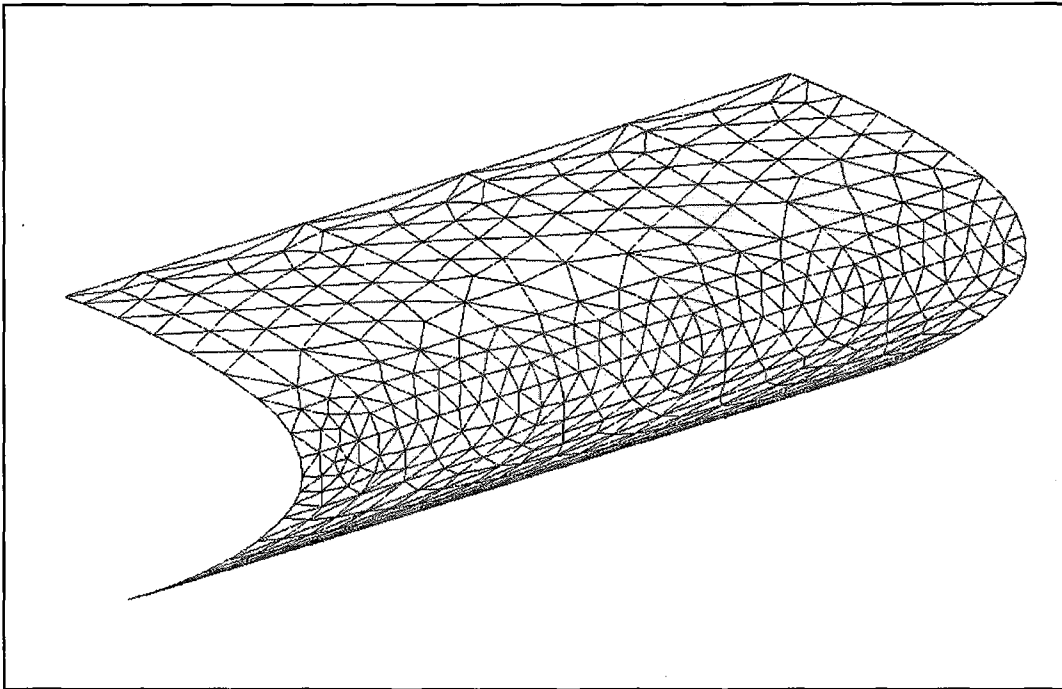


Figure 3.18 Mesh of the leading edge skin

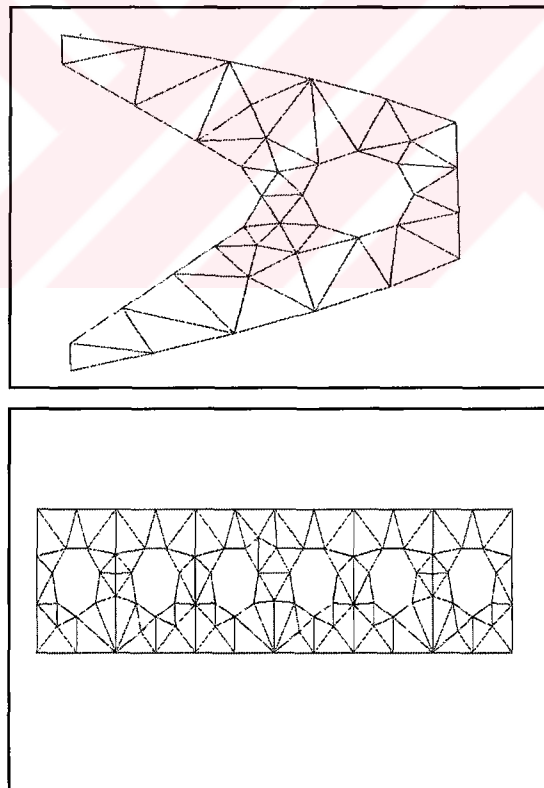


Figure 3.19 Mesh of the leading edge rib and part of the spar

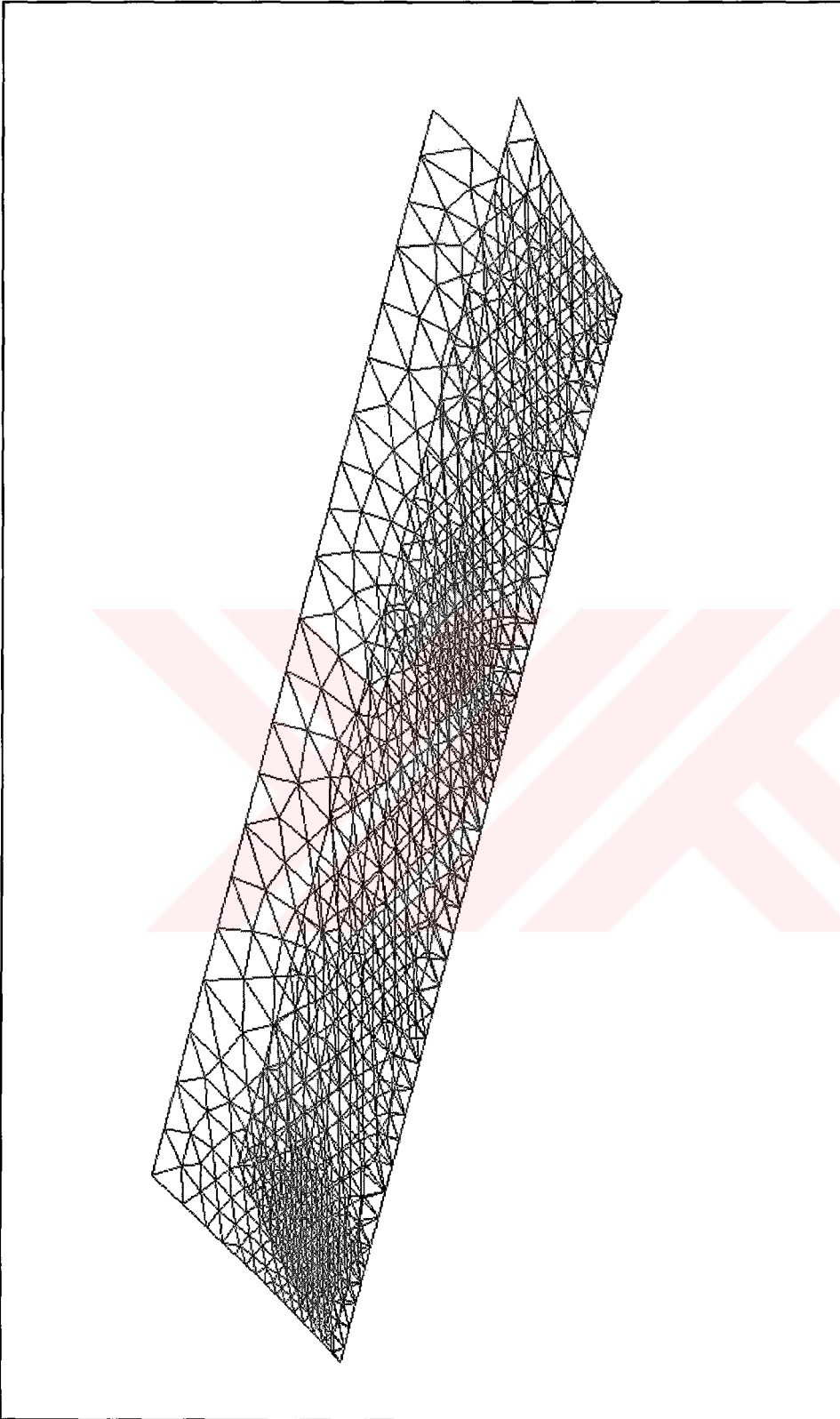


Figure 3.20 Mesh of the inboard and outboard flaps and the aileron trailing edges

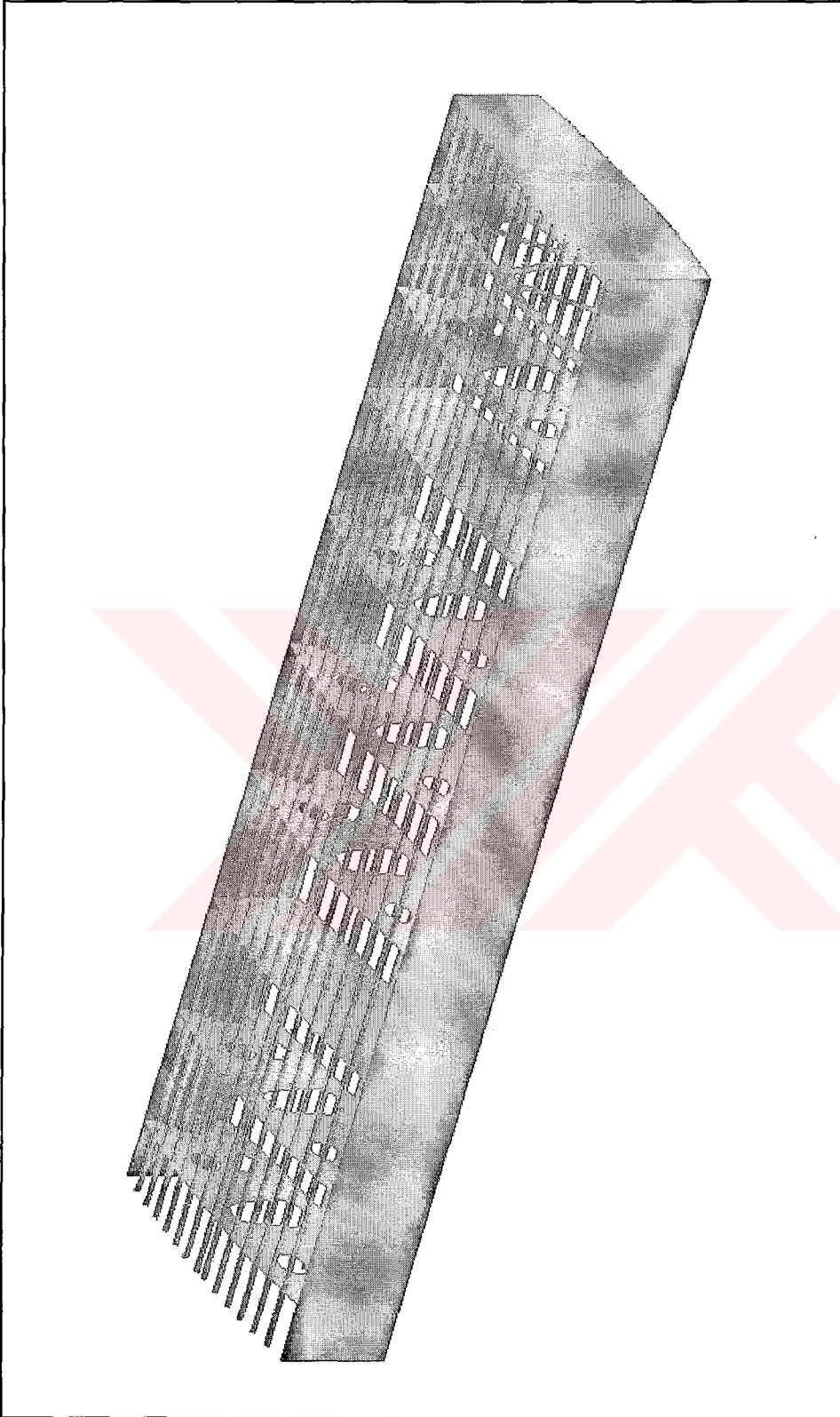


Figure 3.21 Solid view of the mesh of the center wing torque-box with stiffeners

CHAPTER 4

DYNAMIC ANALYSIS OF THE WING

4.1 About Dynamic Analysis Capabilities of I-DEAS

Dynamic analysis routines of the Simulation module of I-DEAS predict the undamped natural frequencies and the natural modes of vibration of a structure. The mode shapes and natural frequencies are useful for the identification of resonance frequencies at which the structure may undergo an undesirably large response to dynamic inputs.

The software solves the mode shapes and resonance frequencies of a finite element model by using three different methods. These are called the Guyan reduction, simultaneous vector iteration (SVI) and Lanczos. Each method has specific advantages over other methods.

Guyan reduction method is non-iterative method, so computer time is more predictable. It is suitable and less expensive for moderate size models with well chosen master degrees of freedom which is used to reduce the DOF that produce the desired modes and frequencies by including only translational DOF. SVI is available for large models and it can be less expensive than Guyan reduction method. In this method there is no need to select master degree of freedom like the Guyan reduction method. Frequency shifting which is used to find the modes near

a certain frequency or to extract modes by shifting the analysis so that mode extraction begins at higher modes or frequencies is also available in simultaneous vector iteration method. Lanczos method has advantages similar to those of SVI and it also can determine the number of modes within the specified frequency range. In this method the accuracy is ensured by a procedure that the number of iterations is automatically determined to achieve the accurate modes. This method is generally faster than SVI. It is recommended by I-DEAS since it is the most commonly used method in industrial applications.

4.2 Normal Mode Dynamic Analyses of the Wing

Lanczos method is used throughout the dynamic analyses of the wing. A verification study of I-DEAS is conducted and presented in Appendix A.

4.2.1 Wing Without Fuel

In this analysis, the primary interest is the determination of the natural frequencies and corresponding mode shapes of the wing having no fuel.

In order to solve the dynamic characteristics of the wing the appropriate boundary conditions must be applied. The boundary condition task of I-DEAS provides tools to create boundary conditions on a finite element model. In an analysis the solver predicts how the model will behave when a set of boundary conditions is applied to it. The restraints, constraints, temperatures and mechanical loads can be applied to model. In order to simulate the real behavior of the wing the elastic boundary conditions can also be specified. Since this is a comparative study basically aimed to determine the change between the characteristics of the wing with and without fuel; the boundary conditions can be chosen as simple as possible in order not to complicate the model and not to increase the solution time. Hence a model with cantilever end conditions will be analyzed. In I-DEAS in order to apply the boundary conditions, the vertices, edges or surfaces can be selected.

After selecting these entities all the nodes and elements related with these entities are also selected. The edges at the root of the wing are selected and all degree of freedoms on the nodes are set to zero to simulate the cantilever end condition. In the analyses whole the structural components and the skin of the wing are considered to be made of an aluminum alloy. Table 4.1 shows the material properties of the typical aluminum alloy used in the aircraft [6].

Table 4.1 Material properties of aluminum alloy used in the analysis

| Aluminum | Material Properties |
|-----------------|--------------------------------|
| Young's Modulus | 70.10^9 [N/m ²] |
| Shear Modulus | 26.10^9 [N/m ²] |
| Yield Strength | 300.10^6 [N/m ²] |
| Density | 2700. [kg/m ³] |

In order to solve any model with normal mode dynamic analysis, a solution set which includes a solution type, a boundary condition set for the analysis, desired output and solution options must be defined. After creating this solution set, the model is ready for dynamic analysis. During the analysis the normal mode dynamics analysis with Lanczos method is selected as a solution type, cantilever end condition at the root of the wing is used as a boundary condition and natural frequencies and mode shapes are obtained as a solver output. After setting the execution options (related with the solution procedure and the files to be listed) the solution is initiated. Finally, the post processing can be used to examine the results.

The first three natural frequencies of flexure for the wing without any fuel are tabulated in Table 4.2 and the corresponding mode shapes are shown in Figures 4.1 to 4.6.

Table 4.2 The natural frequencies for the wing without fuel

| Mode | Natural Frequency [Hz] |
|---------------------------------|------------------------|
| 1 st Bending about Y | 5.65 |
| 1 st Bending about Z | 11.81 |
| 2 nd Bending about Y | 19.84 |



Figure 4.1 Isometric view of the first bending about Y mode shape of the wing without fuel (Deformed and undeformed shapes)



Figure 4.2 Side view of the first bending about Y mode shape of the wing without fuel (Deformed and undeformed shapes)



Figure 4.3 Isometric view of the first bending about Z mode shape of the wing without fuel (Deformed and undeformed shapes)



Figure 4.4 Top view of the first bending about Z mode shape of the wing without fuel (Deformed and undeformed shapes)

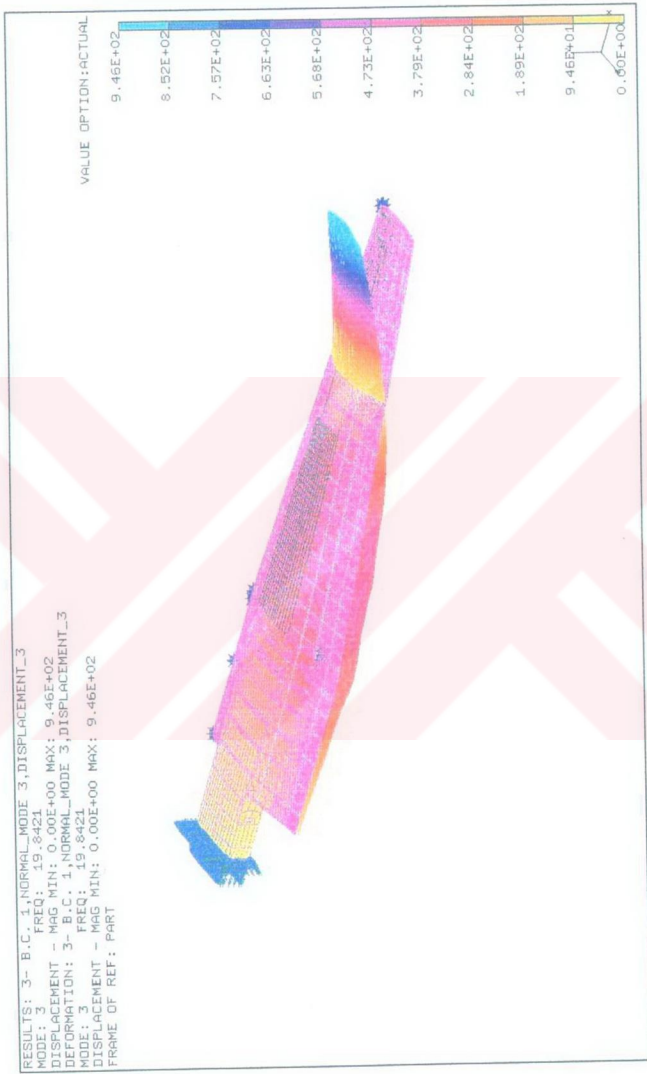


Figure 4.5 Isometric view of the second bending about Y mode shape of the wing without fuel (Deformed and undeformed shapes)



Figure 4.6 Side view of the second bending about Y mode without fuel (Deformed and undeformed shapes)

4.2.2 Wing With Fuel

In this section, the dynamic analysis of the wing having fuel is performed and the natural frequencies and corresponding mode shapes are determined.

The critical part of the analysis is the modeling of the effect of the fuel on the wing. Throughout the analysis the fuel is considered as lumped masses between the station numbers 1100 and 3100 for the center wing and between the station numbers 4250 and 8110 for the outer wing. As previously described the station numbers are the distances measured from the center line of the wing in millimeters. In the center wing, there are 5 ribs between the stations 1100 and 3100 and in the outer wing, there are 9 ribs between the stations 4250 and 8110. Figure 4.7 represents the location of the fuel and the station numbers of the center and the outer wing ribs.

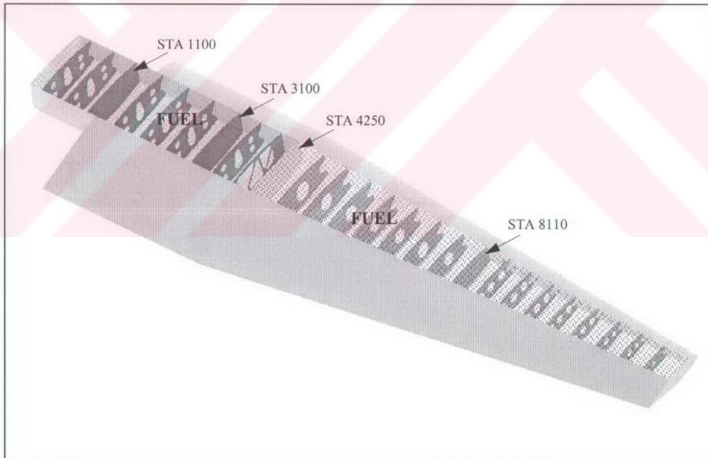


Figure 4.7 The location of the fuel and the station numbers of the ribs

Altogether 14 ribs are considered and for each rib 4 nodes are created. Figure 4.8 shows the location of the lumped mass elements on a rib. These nodes are used for the lumped mass elements and the whole surface mesh for these ribs are regenerated. Figure 4.9 and Figure 4.10 show the new mesh using lumped mass elements for two selected ribs. In order to determine the values of the lumped masses, the center and the outer wing ribs and the corresponding fuel weights are considered separately. The fuel capacities of the center and the outer wing are 836.6 kg and 845.4 kg respectively.

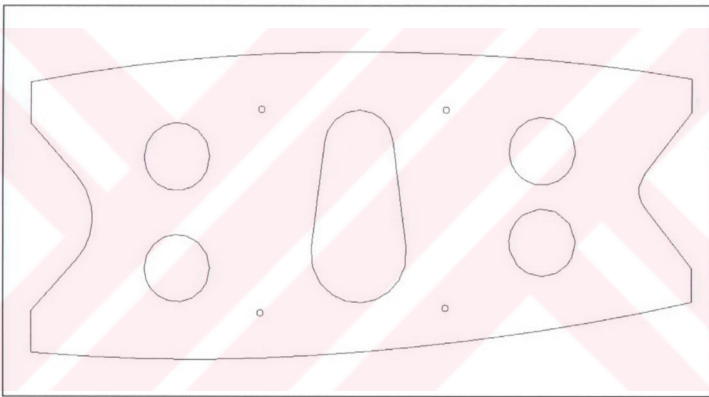


Figure 4.8 The location of the lumped mass elements on a rib

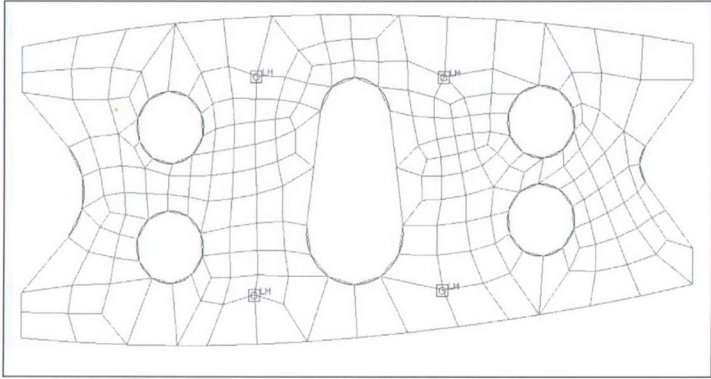


Figure 4.9 The new mesh generated with lumped mass and shell elements
(a rib with holes)



Figure 4.10 The new mesh generated with lumped mass and shell elements
(a rib without any hole)

In the center wing there are 5 ribs containing four nodes and in the outer wing there are 9 ribs also containing four nodes. This totally results 20 nodes and 36 nodes for the center and the outer wing respectively. If 836.6 kg is divided to 20 and 845.4 kg is divided to 36, the results are the lumped mass values which will be applied to each node for the mass modeling of fuel. Thus, the lumped mass element must be created in such a way that 41.83 kg is applied to each node on the center wing ribs and 23.48 kg is applied to each node on the outer wing ribs.

In the solution of the wing with fuel the method, boundary condition and the solution output are the same as those used in the wing having no fuel. The natural frequencies are tabulated in Table 4.3 and corresponding mode shapes of the wing with fuel are shown in Figures 4.11 to 4.16.

Table 4.3 The natural frequencies for the wing with fuel

| Mode | Natural Frequency [Hz] |
|---------------------------------|------------------------|
| 1 st Bending about Y | 3.51 |
| 1 st Bending about Z | 6.92 |
| 2 nd Bending about Y | 13.27 |



Figure 4.11 Isometric view of the first bending about Y mode shape of the wing with fuel (Deformed and undeformed shapes)



Figure 4.12 Side view of the first bending about Y mode shape of the wing with fuel (Deformed and undeformed shapes)

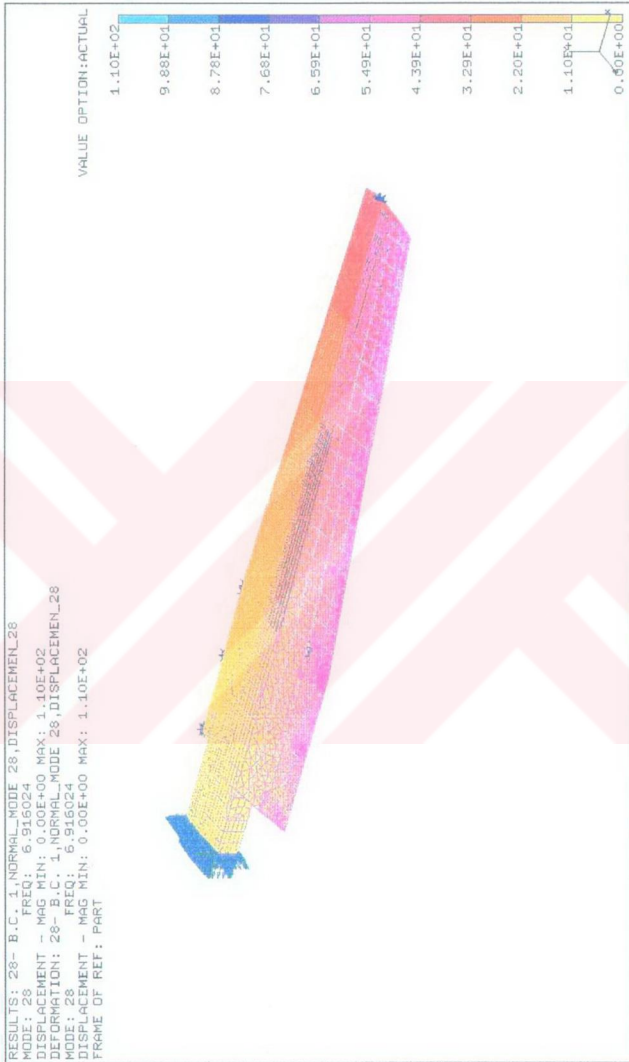


Figure 4.13 Isometric view of the first bending about Z mode shape of the wing with fuel (Deformed and undeformed shapes)

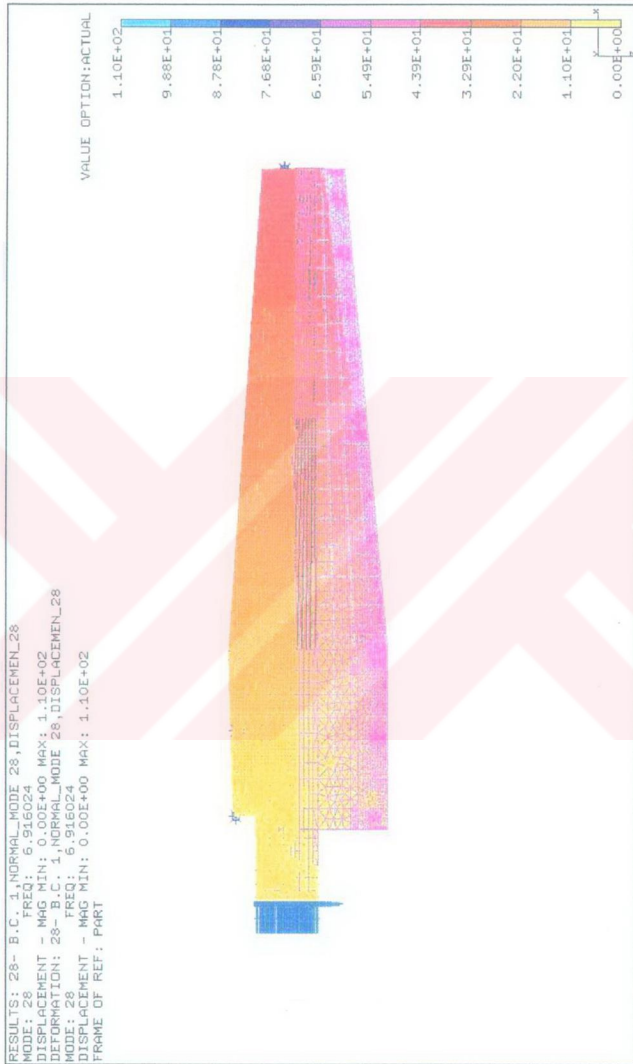


Figure 4.14 Top view of the first bending about Z mode shape of the wing with fuel (Deformed and undeformed shapes)

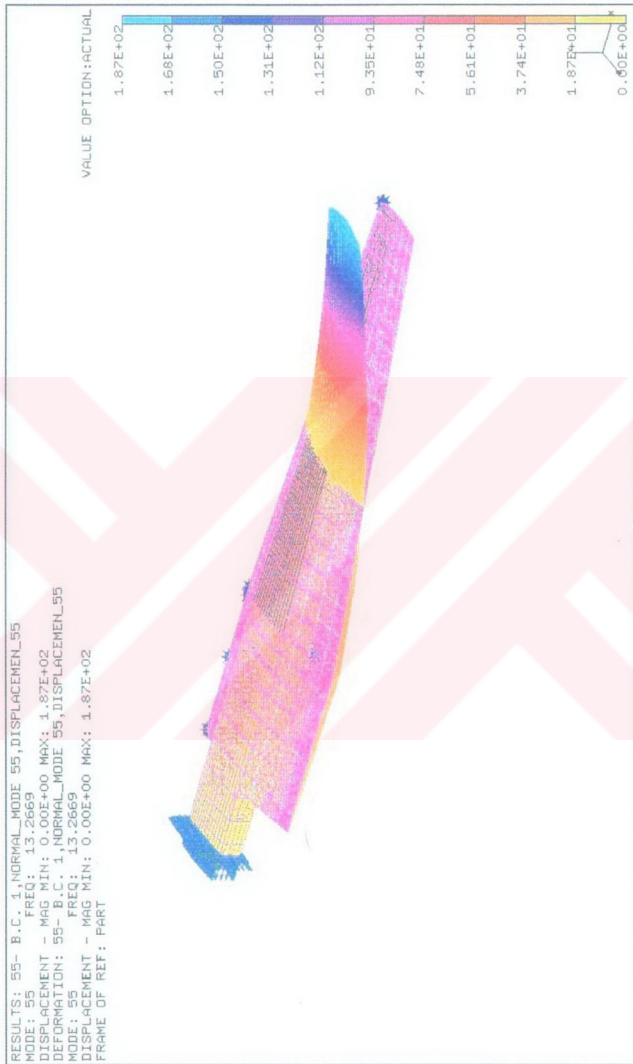


Figure 4.15 Isometric view of the second bending about Y mode shape of the wing with fuel (Deformed and undeformed shapes)

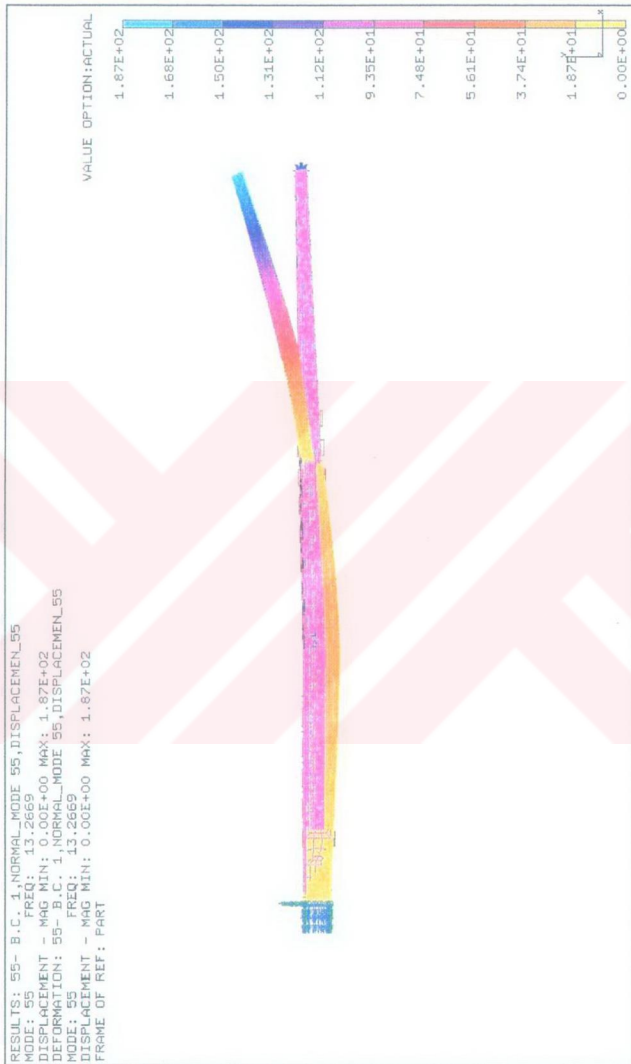


Figure 4.16 Side view of the second bending about Y mode shape of the wing with fuel (Deformed and undeformed shapes)

After finding the natural frequencies of the wing for with and without fuel cases Table 4.4 is obtained. It shows the percentage difference between the two cases in order to investigate the fuel effect. The reduction means that there is a decrease in natural frequencies of the wing.

Table 4.4 The percentage difference between the natural frequencies of the wing with fuel and without fuel

| Mode | Percentage Difference in Natural Frequency |
|---------------------------------|--|
| 1 st Bending about Y | 37.88 % (reduction) |
| 1 st Bending about Z | 41.41 % (reduction) |
| 2 nd Bending about Y | 33.11 % (reduction) |

As it can be seen from Table 4.4, all the natural frequencies of the wing with fuel case turns out to be lower than those of the wing without fuel case because of the lumped mass effect.

The addition of the mass to any structure decreases the natural frequencies [7]. This expected situation also occurs in the wing model with fuel case. Therefore, it can also be considered as a verification of the wing model.

CHAPTER 5

STATIC ANALYSIS OF THE WING

5.1 About Linear Static Analysis Capabilities of I-DEAS

The linear static analysis routines predict the static behavior of a structure which has forces applied on it and solves for displacements and stresses of a finite element model. The behavior of the structure is characterized by its displacement. If the displacement of a structure is known, other relevant data such as stresses can be calculated from it. Additionally the types of output that can be stored or listed for linear static analysis include reaction forces, strains, strain energies, element forces, shell stress, resultant stress and strain at integration points and element strain energy error. The solver can also analyze contact between surfaces or element faces.

The software solves these outputs by using three different method. These are called the linear static p-method, linear static adaptive method and linear static method. Each method has specific characteristics and application areas.

The linear static p-method is a linear statics solver that uses polynomial order of a fixed mesh of solid, tetrahedron elements to control the accuracy. The conventional finite element method reduces the error of approximation (or discretization error) of the solution by refining the mesh. This method generally

uses elements that introduce additional nodes to increase the accuracy. The p-method reduces the discretization error by using elements formulated with a polynomial order that can be increased systematically to a higher order. These elements (known as p-elements) have their polynomial order increased by adding degrees of freedom that are not nodally based p-element meshes are created by using the solid parabolic tetrahedrons. The most important benefit of the p-method is that it can provide very accurate results with a minimum of user interaction. In addition to its accuracy, the p-method can estimate solution error. This method is most useful when one can adequately represent the geometry of a structure with a reasonably coarse mesh and when nonlinear behavior is not a concern. The software allows one to perform various types of p-method solutions including adaptive p and uniform p analyses. Uniform p analysis uniformly increases the p order of every element in the model up to the specified p order. On the other hand adaptive p analysis increases the p order only where necessary in the model. Therefore, it is faster and uses less disk space than uniform p while still providing very accurate results.

Linear statics adaptive analysis on the other hand can perform a linear statics solve and adaptive meshing as one process from the I-DEAS Model Solution software. Linear statics adaptive analysis iteratively performs linear elastic analysis and adaptive meshing without user intervention. When linear statics adaptive analysis is run, the solver initially performs linear statics analysis on the model. Then, based on the energy error norm results of the solution, the software determines if the solution is converged. The solver repeats adaptive meshing and linear statics analysis until results converge to the desired accuracy or until the specified number of iterations of adaptive meshing/solving have been completed. The software creates an intermediate model for each new mesh created by adaptive meshing. It then solves this new model. After each solution is completed, the software saves the intermediate model containing the current mesh. The adaptive meshing can reduce elemental distortion in the model and refine a mesh in areas where error estimates are highest. The adaptive meshing capability automatically improves a mesh by completely remeshing the model.

In the static analysis of the wing since there is no solid elements and the mesh is generated in such a way that all the element lengths are considered to obtain as fine mesh as possible, the p-method is not used. Furthermore, when using the linear statics adaptive analysis the model must be constructed only from a single family of elements, that is there is no permission to mix the element families. For this reason the linear statics adaptive method can not also be selected for the analysis. Therefore, throughout the analysis the linear static analysis is used.

In order to solve any model with linear static analysis, at first, a solution set including the solution type (for this analysis it is linear static), boundary condition set (cantilever end condition), solution option and output (displacements and stresses) must be defined. Next, the execution options (related with the solution procedure and the files to be listed) are selected and the solution is initiated. Finally, the post processing can be used to examine the results.

In the results of the static analysis the results are presented with the following units.

Displacement : [mm]

Stress : [mN/mm²]

5.2 Application of g-Loading

Loads are the forces that bear on a body. In I-DEAS one can apply four types of loads: gravity, motion (acceleration), force, and initial condition (displacement and/or velocity). Gravity is a vector of distributed and constant body force. In order to define gravity as a boundary condition, one can define a vector (direction) and a magnitude which are multiplied to yield the acceleration used by the solver. The vector is entered in global coordinates. By default, the scale factor is 1 and the value for the vector is (0, -9.8, 0). This yields an acceleration of

(0, 9.8, 0) aligned with the negative Y axis. On the other hand, g-loading can also be applied to the model in more than one direction by properly defining the magnitude and the direction of the components of the g vector.

In this section the wing is analyzed first by considering its own weight. Both with and without fuel cases are studied. Then, another analysis is performed for a multi-directional g-loading. In that the maximum possible g-loads that a typical aircraft of this class is subjected to are found from military standards. Then a worst possible case is determined by the simultaneous application of those loads. Since those loads are typical flight loads, the analysis is only conducted for a wing having fuel.

5.2.1 Analysis of the Wing Under Its Own Weight

The static analysis of the wing under its own weight is performed by taking $g = 1$. That corresponds to an acceleration of -9.8 m/s^2 in the negative Y direction in global coordinates. The boundary condition is again cantilever like the dynamic analysis. After applying the g-loading to the wing, the displacement and the Von Mises stress values are obtained for the wing with fuel and without fuel cases. The isometric view of the displacement and the Von Mises stress values of the wing under its own weight without any fuel can be seen from the Figures 5.1 and 5.2. Figures 5.3. and 5.4 show the same view that of the wing by considering the fuel effect. It was determined that there was an increase in the displacement and stress values due to the added fuel. The percentage differences of the two cases are shown in Table 5.1

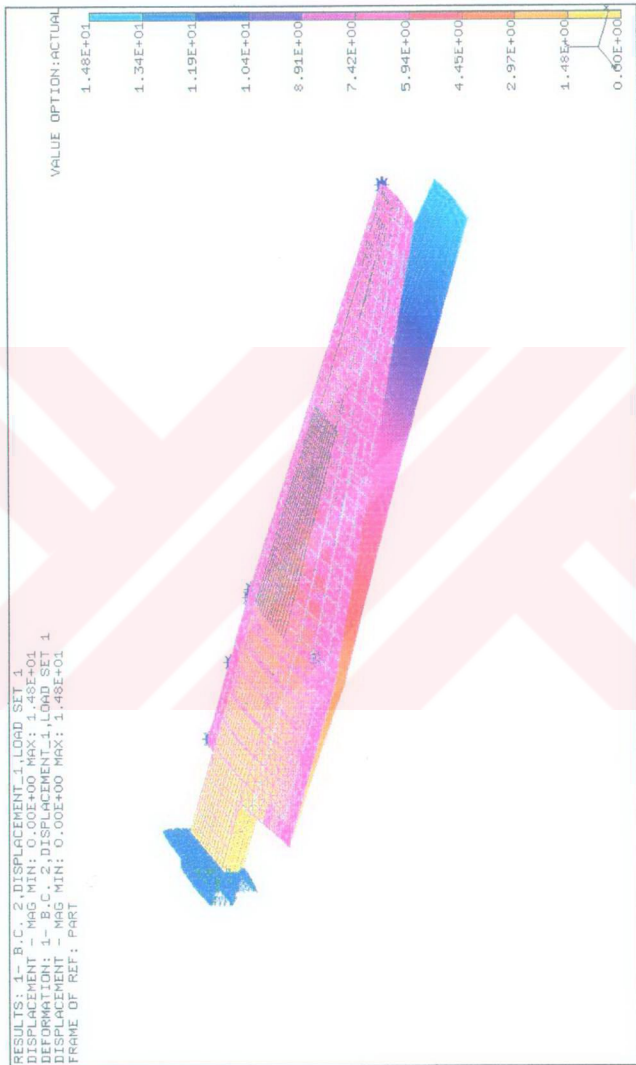


Figure 5.1 Isometric view of the total displacement pattern of the wing without fuel under its own weight

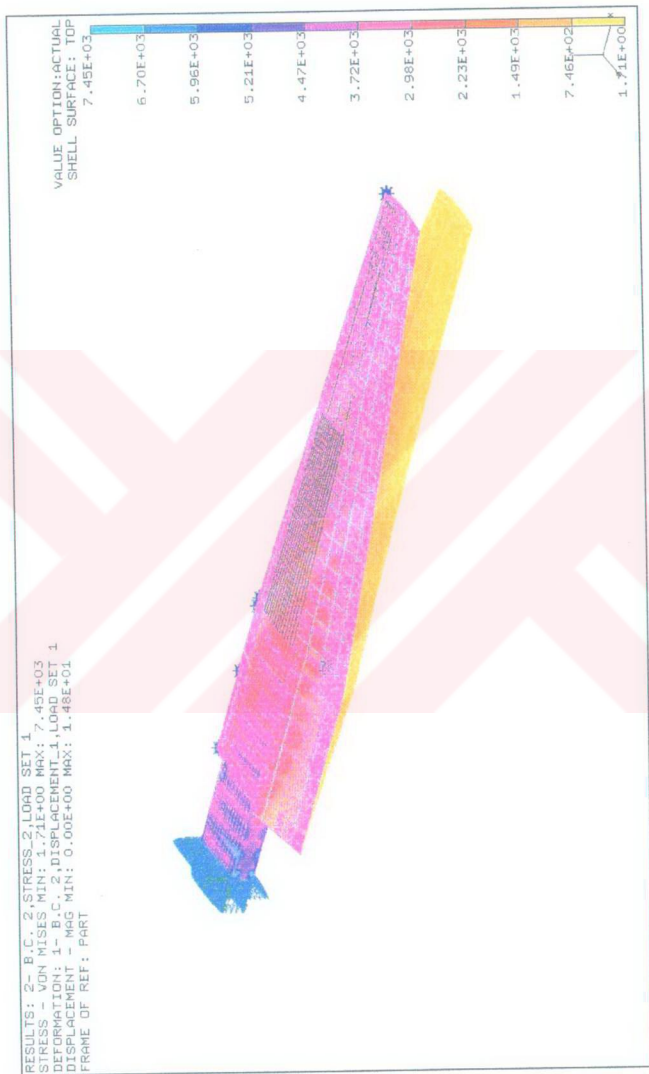


Figure 5.2 Isometric view of the Von Mises stress distribution of the wing without fuel under its own weight

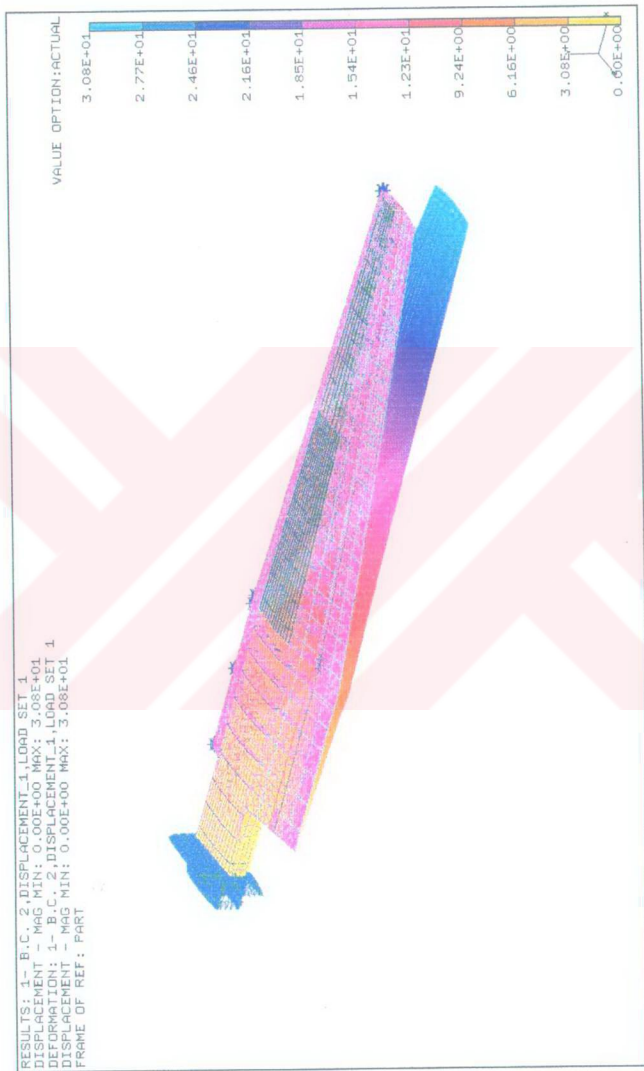


Figure 5.3 Isometric view of the total displacement pattern of the wing with fuel under its own weight

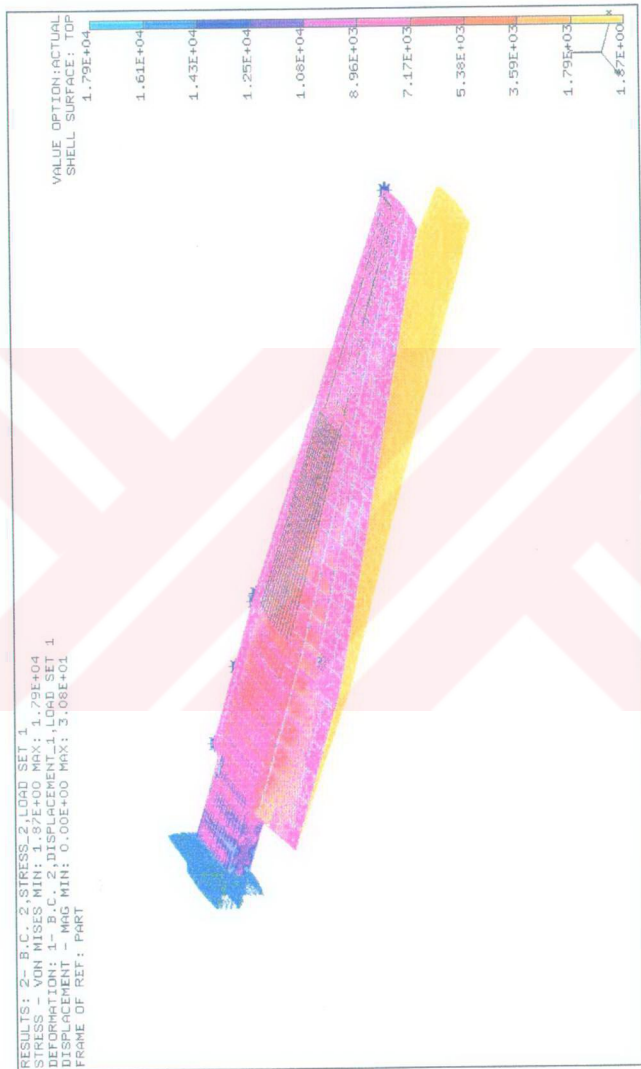


Figure 5.4 Isometric view of the Von Mises stress distribution of the wing with fuel under its own weight

Table 5.1 The percentage difference between the maximum displacement and the maximum Von Mises Stress for the wing with fuel and without fuel

| | Percentage Difference |
|--------------------------|-----------------------|
| Maximum Displacement | 51.95 % |
| Maximum Von Mises Stress | 58.38 % |

5.2.2 Analysis of the Wing Under Various g-Loading

The structural loads that are induced on the aircraft structures by the in-service accelerations are given in Military Standard MIL-STD-810E [8]. Table 5.2 indicates the suggested g levels for an aircraft of type under consideration. Figure 5.5 shows the isometric view of the wing subjected to g vector.

Table 5.2 Typical maximum g values for the aircraft

| Direction of the G Vector | G Value |
|---------------------------|---------|
| X (Aft) | 4.5 |
| Y (Up) | 6.75 |
| Z (Lateral Right) | 3 |

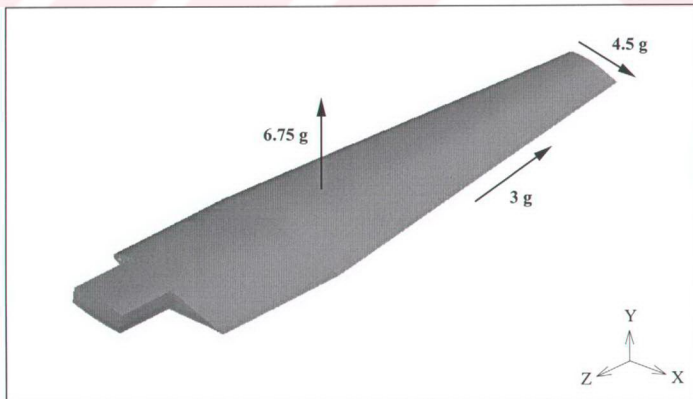


Figure 5.5 G-loading vector components on isometric view of the wing

In this section, by considering those g values, the total displacement and the Von Mises stresses are investigated.

Figures 5.6 to 5.8 show the displacement patterns of the wing with isometric, side and the top views. The Von Mises stress distribution on the wing is given in Figure 5.9. It can be seen that the higher stresses occur near cantilever end. Figure 5.10 represents the isometric zoom view of the Von Mises stress distribution near the root of the wing with fuel.

5.3 Determination of the Effective Transverse Stiffnesses of the Wing

In this section the static behavior of the wing is analyzed under different loading conditions. A point force of varying magnitude is applied at the tip of the wing in positive and negative global Y and Z directions. The resulting displacement patterns and the Von Mises stress distributions of the wing are obtained.

It is determined that the force applied in positive Y direction gives an absolute maximum displacement value same as the force applied in negative Y direction and the force applied in positive Z direction results in the same absolute maximum displacement value of the force applied in negative Z direction. Hence only the displacements resulting from the forces applied in positive directions are considered and the figures are drawn obtained by considering the results of these positive forces. Figures 5.11 and 5.12 show the force versus displacement curves for those cases.



Figure 5.6 Isometric view of the total displacement pattern of the wing under various g-loading



Figure 5.7 Side view of the total displacement pattern of the wing under various g-loading

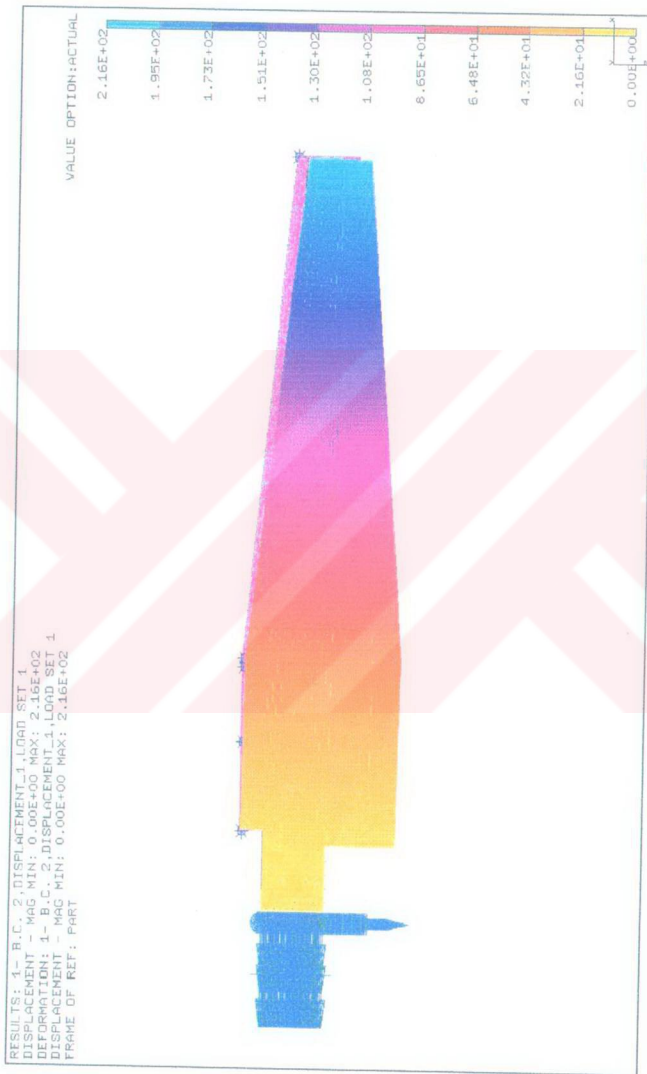


Figure 5.8 Top view of the total displacement pattern of the wing under various g loading



Figure 5.9 Isometric view of the Von Mises stress distribution of the wing under various g-loading



Figure 5.10 Isometric zoom view of the Von Mises stress distribution of the wing near root under various g-loading

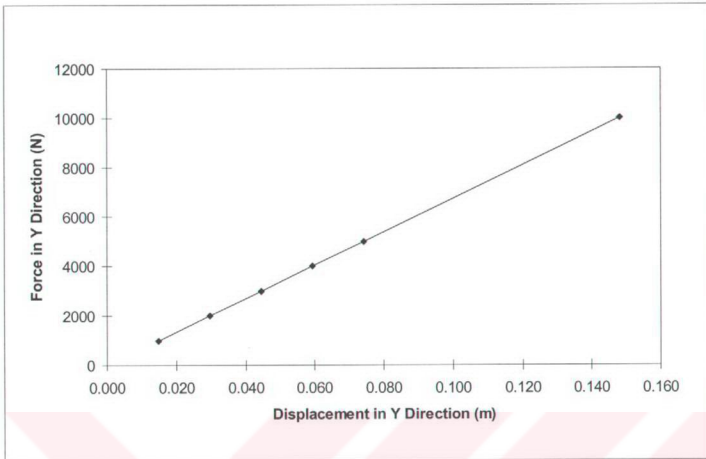


Figure 5.11 Force versus displacement curve in Y direction

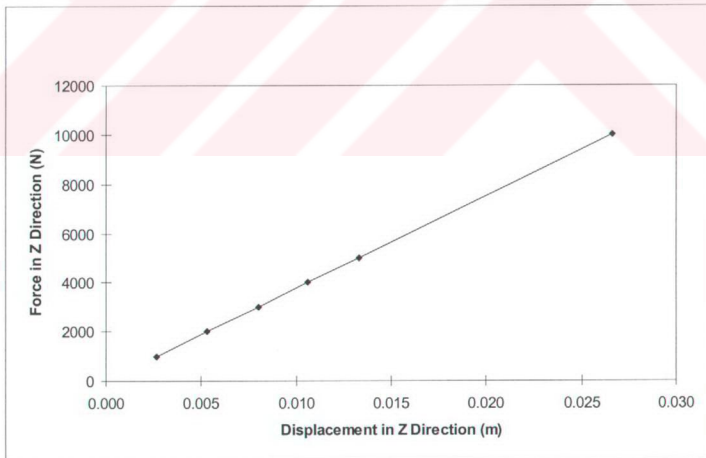


Figure 5.12 Force versus displacement curve in Z direction

As it can be seen from Figures 5.11 and 5.12 that there is a linear behavior between the applied force and the resulting displacement in the direction of the applied force. The slope of the curves give the effective transverse stiffness of the wing in global Y and Z directions respectively. Table 5.3 presents the effective stiffness of the wing in those directions and yields that the wing under consideration is stiffer in Z direction.

Table 5.3 Effective stiffnesses of the wing

| Direction | Effective Stiffness [N/m] |
|-----------|---------------------------|
| Y | $67.57 \cdot 10^3$ |
| Z | $375.94 \cdot 10^3$ |

The resulting displacement patterns and the Von Mises stress distributions of the wing corresponding to the maximum load of 10 kN are shown in Figures 5.13 to 5.18.

A comparison of Figures 5.15 and 5.18 yields that lower stresses are developed in F_z application because of higher transverse stiffness in Z direction.



Figure 5.13 Isometric view of the total displacement pattern of the wing under a force of $F_y = 10000$ N



Figure 5.14 Side view of the total displacement pattern of the wing under a force of $F_y = 10000$ N



Figure 5.15 Isometric view of the Von Mises stress distribution of the wing under a force of $F_y = 10000\text{ N}$

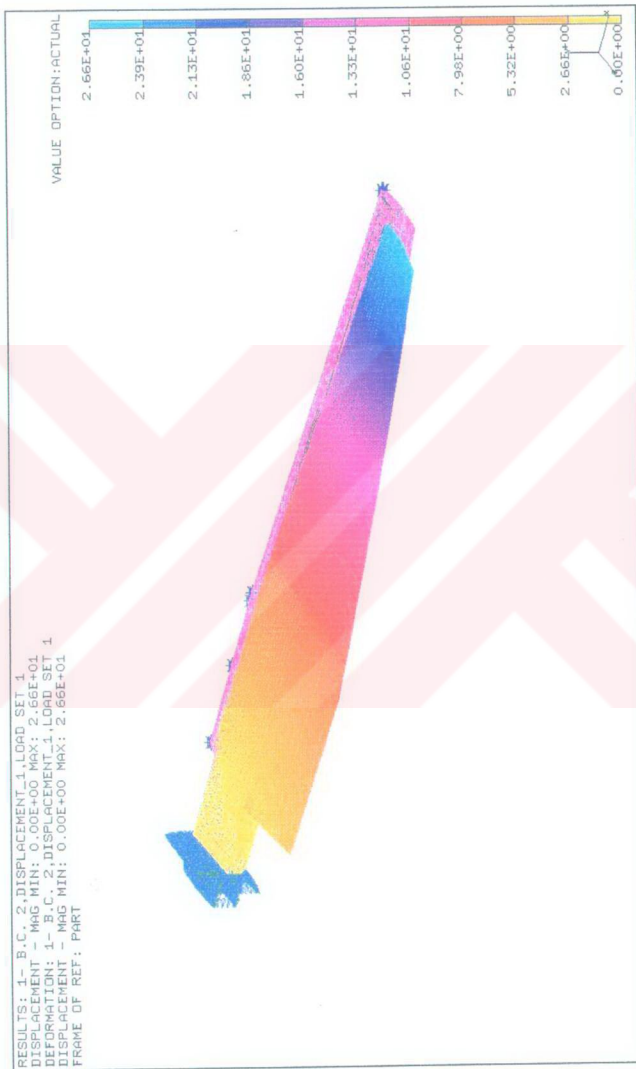


Figure 5.16 Isometric view of the total displacement pattern of the wing under a force of $F_z = 10000$ N

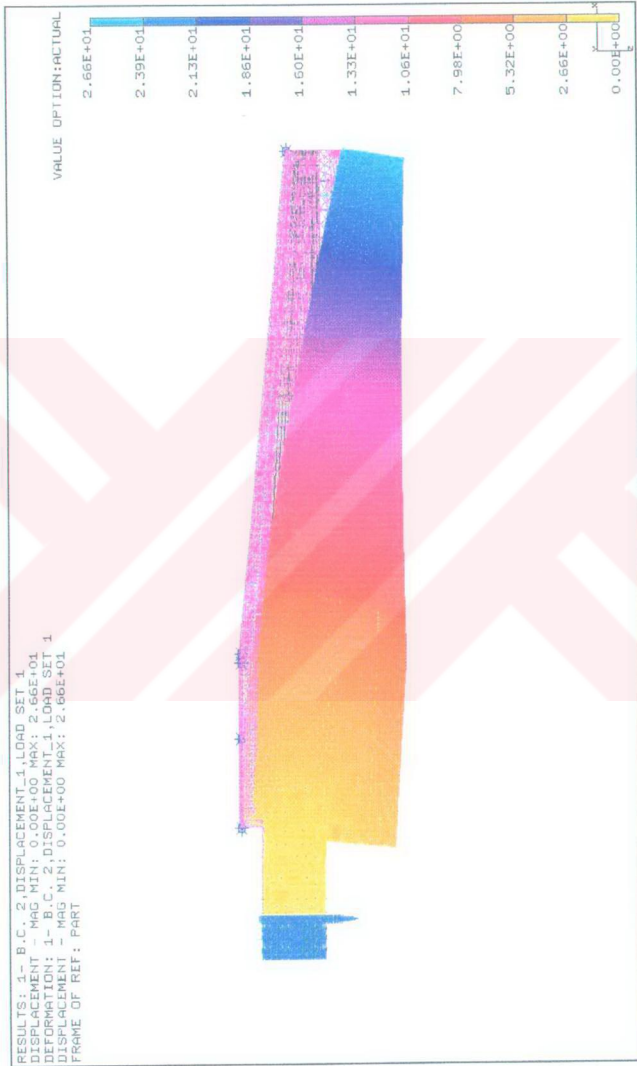


Figure 5.17 Top view of the total displacement pattern of the wing under a force of $F_z = 10000\text{ N}$

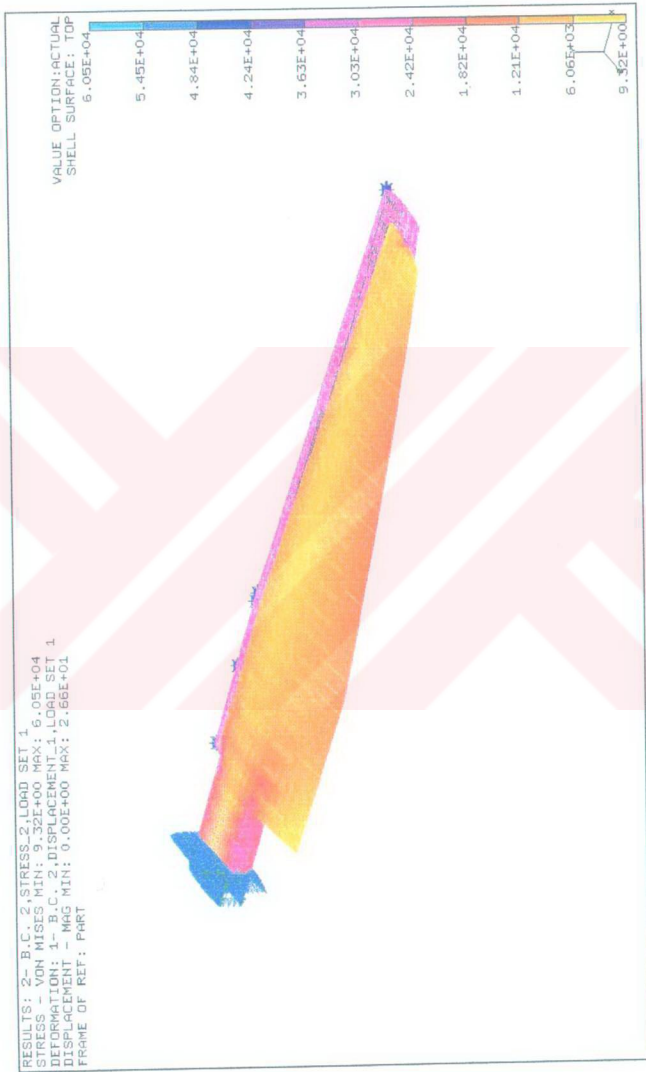


Figure 5.18 Isometric view of the Von Mises stress distribution of the wing under a force of $F_z = 10000$ N

CHAPTER 6

CONCLUSIONS

In this study, the structural characteristics of a medium-range transport aircraft wing was investigated with the help of a package program called I-DEAS.

A dynamic analysis which is aimed to find the natural frequencies and the corresponding mode shapes of the wing and a static analysis for the determination of stress and displacement patterns were performed. The results were tabulated and compared for with and without fuel cases.

In the determination of the dynamic characteristics of the wing, all the natural frequencies of the wing with fuel turns out to be lower than those of the wing without fuel. This expected result can be considered as a verification of the developed wing model. The analyses conducted for the investigation of the g-loading effect show that there are increases in the displacement and stress values due to the added fuel. It has also been determined that the wing considered is stiffer about Y axis than Z axis. Furthermore, in all the cases considered, no failure of the wing is observed under the applied loading.

The studied model which is created to simulate the wing can be improved in many ways. First a much more detailed model can be constructed by drawing all the components of the wing including the connecting mechanism of the flaps and

the aileron, stiffeners of the ribs and flaps even rivets for detailed analysis. Furthermore more realistic elastically supported end boundary conditions can be applied. In addition to those all the components can be meshed by using their real material properties such as the composite material can be used for the skin of the flaps and the aileron. A much finer mesh can also be generated on the model either by using small brick elements or by reducing the element length of the previously defined mesh. But this modification requires a higher performance computer with relevant hardware since the reduction in mesh size greatly increases the solution time.

Finally it can be said that the model of the wing is only a small part of the complete aircraft model. The inclusion of the fuselage and the control surfaces will definitely make the analysis more realistic and will give more information about the structural characteristics and the behavior of the aircraft. Nevertheless it is believed that the present study opens a way for more complicated analyses.

REFERENCES

1. I-DEAS Design Reference Guide, Release 6,
Structural Dynamics Research Corporation (SDRC®), August 1998
2. I-DEAS Simulation, Model Solution/Optimization User's Guide, Release 6,
Structural Dynamics Research Corporation (SDRC®), August 1998
3. I-DEAS Simulation, Element Library, Release 6,
Structural Dynamics Research Corporation (SDRC®), August 1998
4. J. N. Reddy, "An introduction to the Finite Element Method", Second Edition
McGraw-Hill Book Company, 1993
5. I-DEAS Simulation, Finite Element Modeling User's Guide, Release 6,
Structural Dynamics Research Corporation (SDRC®), August 1998
6. David J. Peery, J. J. Azar, "Aircraft Structures",
McGraw-Hill Book Company, 1982
7. Robert D. Blevins, "Formulas for Natural Frequency and Mode Shape",
Litton Educational Publishing, Inc., 1979
8. Military Standard MIL-STD-810E

APPENDIX A

VERIFICATION OF DYNAMIC ANALYSIS CAPABILITIES OF I-DEAS

In order to verify the dynamic analysis capabilities of I-DEAS, a clamped-free uniform aluminium beam is selected. Figure A.1 gives the beam and its dimensions. The first ten natural frequencies of the beam is analytically obtained. Those frequencies include the first ten natural frequencies in turn being flexural, torsional and axial frequencies. Table A.1 gives the material properties and Table A.2 shows the first ten natural frequencies with appropriate characteristics. In theoretical calculations the Timoshenko beam theory with only shear deformation characteristics and non-circular beam torsion theory are used.

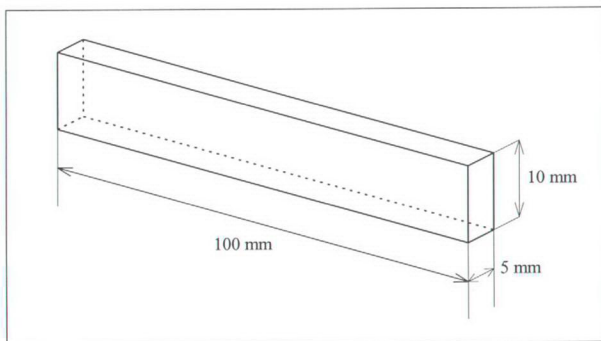


Figure A.1 Beam used in the analyses and its dimensions

Table A.1 Material properties of aluminium used in the analyses

| Aluminium | Material Properties |
|-----------------|-------------------------------|
| Young's Modulus | 70.10^9 [N/m ²] |
| Shear Modulus | 26.10^9 [N/m ²] |
| Density | 2700. [kg/m ³] |

Table A.2 First ten theoretical natural frequencies of the beam

| Mode | Natural Frequency [Hz] |
|---------------------------------|------------------------|
| 1 st Bending about Y | 410.46 |
| 1 st Bending about Z | 815.99 |
| 2 nd Bending about Y | 2540.59 |
| 2 nd Bending about Z | 4878.14 |
| 1 st Torsional | 5746.79 |
| 3 rd Bending about Y | 6978.27 |
| 1 st Axial | 12729.38 |
| 3 rd Bending about Z | 12790.11 |
| 4 th Bending about Y | 13316.41 |
| 2 nd Torsional | 17240.38 |

In the dynamic analysis of I-DEAS, three different element types are used with various element sizes by using Lanczos method.

Table A.3 First ten natural frequencies of the beam by using tetrahedron solid elements with element length of 2 (Number of nodes : 9058, Number of elements: 5309)

| Mode | Natural Frequency [Hz] |
|---------------------------------|------------------------|
| 1 st Bending about Y | 413.24 |
| 1 st Bending about Z | 819.86 |
| 2 nd Bending about Y | 2558.74 |
| 2 nd Bending about Z | 4911.01 |
| 1 st Torsional | 5755.69 |
| 3 rd Bending about Y | 7035.46 |
| 1 st Axial | 12770.11 |
| 3 rd Bending about Z | 12911.36 |
| 4 th Bending about Y | 13446.85 |
| 2 nd Torsional | 17287.55 |

Table A.4 First ten natural frequencies of the beam by using tetrahedron solid elements with element length of 3 (Number of nodes : 3045, Number of elements: 1600)

| Mode | Natural Frequency [Hz] |
|---------------------------------|------------------------|
| 1 st Bending about Y | 413.71 |
| 1 st Bending about Z | 820.13 |
| 2 nd Bending about Y | 2561.07 |
| 2 nd Bending about Z | 4911.34 |
| 1 st Torsional | 5719.81 |
| 3 rd Bending about Y | 7040.68 |
| 1 st Axial | 12772.48 |
| 3 rd Bending about Z | 12908.21 |
| 4 th Bending about Y | 13453.91 |
| 2 nd Torsional | 17153.08 |

Table A.5 First ten natural frequencies of the beam by using quadrilateral thin shell elements with element length of 1 (Number of nodes : 1111, Number of elements: 1000)

| Mode | Natural Frequency [Hz] |
|---------------------------------|------------------------|
| 1 st Bending about Y | 412.51 |
| 1 st Bending about Z | 817.29 |
| 2 nd Bending about Y | 2560.95 |
| 2 nd Bending about Z | 4898.03 |
| 1 st Torsional | 6439.39 |
| 3 rd Bending about Y | 7068.85 |
| 1 st Axial | 12749.43 |
| 3 rd Bending about Z | 12886.22 |
| 4 th Bending about Y | 13577.39 |
| 2 nd Torsional | 19325.89 |

Table A.6 First ten natural frequencies of the beam by using quadrilateral thin shell elements with element length of 3 (Number of nodes : 136, Number of elements: 99)

| Mode | Natural Frequency [Hz] |
|---------------------------------|------------------------|
| 1 st Bending about Y | 412.69 |
| 1 st Bending about Z | 817.57 |
| 2 nd Bending about Y | 2560.90 |
| 2 nd Bending about Z | 4899.30 |
| 1 st Torsional | 6004.36 |
| 3 rd Bending about Y | 7068.34 |
| 1 st Axial | 12752.12 |
| 3 rd Bending about Z | 12892.80 |
| 4 th Bending about Y | 13578.44 |
| 2 nd Torsional | 18002.67 |

Table A.7 First ten natural frequencies of the beam by using beam elements with element length of 1 (Number of nodes : 101, Number of elements: 100)

| Mode | Natural Frequency [Hz] |
|---------------------------------|------------------------|
| 1 st Bending about Y | 410.42 |
| 1 st Bending about Z | 815.88 |
| 2 nd Bending about Y | 2541.33 |
| 2 nd Bending about Z | 4884.37 |
| 1 st Torsional | 5750.18 |
| 3 rd Bending about Y | 6984.33 |
| 1 st Axial | 12729.51 |
| 3 rd Bending about Z | 12829.05 |
| 4 th Bending about Y | 13338.36 |
| 2 nd Torsional | 17251.98 |

Tables A.2 to A.7 indicate that the results of I-DEAS runs are close to the theoretical ones. Further comparison of Tables A.3 and A.7 show that the accuracy gained in the solid element case is not very significant despite the higher number of nodes and elements introduced. Therefore in order to avoid longer solution time and larger solution space, in the analysis of actual wing model the utilization of solid elements is completely avoided. The panels are modelled with shell elements and beam-like structures are modelled by using appropriate section beam elements.

APPENDIX B

PRESENTATION OF HARDWARE AND MODELING ASPECTS

The hardware used during the analyses has the following properties;

| | |
|--------------------------|--|
| Workstation Type | : HP 9000 J 2240 series |
| Operating System | : HP-UX version 10.20 ACE plus J2240 Hardware Extensions Software |
| User Interface | : HP VUE version 3.0 Graphical User Interface |
| Main Memory | : 2.1 GB with two processors |
| Internal Software Device | : 10 GB Hard Disk Drive, CD-ROM Drive, 4 mm DDS Tape Drive |

This part gives the results of selected dynamic and static analysis runs with corresponding time and space requirements. In the dynamic analysis the first twenty natural frequencies and mode shapes (both local and global values) of the wing are considered for with and without fuel cases. In the static analysis, the behavior of the wing under its own weight is considered again for with and without fuel cases.

Table B.1 Dynamic Analysis of the wing without fuel (First 20 modes)

| | |
|-------------------------------------|----------------|
| Number of nodes | 18543 |
| Number of elements | 32809 |
| Memory used by sparse matrix solver | 184 MB |
| Estimated decomposition time | 48 cpu seconds |
| Size of scratch files | 316 MB |

Table B.2 Dynamic Analysis of the wing with fuel (First 20 modes)

| | |
|-------------------------------------|----------------|
| Number of nodes | 18544 |
| Number of elements | 32866 |
| Memory used by sparse matrix solver | 183 MB |
| Estimated decomposition time | 56 cpu seconds |
| Size of scratch files | 208 MB |

Table B.3 Static Analysis of the wing under its own weight without fuel

| | |
|-------------------------------------|----------------|
| Number of nodes | 18543 |
| Number of elements | 32809 |
| Memory used by sparse matrix solver | 166 MB |
| Estimated decomposition time | 56 cpu seconds |
| Size of scratch files | 20 MB |

Table B.4 Static Analysis of the wing under its own weight with fuel

| | |
|-------------------------------------|----------------|
| Number of nodes | 18544 |
| Number of elements | 32866 |
| Memory used by sparse matrix solver | 166 MB |
| Estimated decomposition time | 56 cpu seconds |
| Size of scratch files | 20 MB |

